Characterizing Aerosol Emissions from Biomass Burning

Muhammad Anupam Shaikat
EES-2019-355

Master Programme Energy and
Environmental Sciences, University of Groningen

Research report of Muhammad Anupam Shaikat

Report: EES-2019-355

Supervised by:
Prof. dr. Ulrike Dusek, CIO
Prof. dr. Harro Meijer, CIO

University of Groningen
Energy and Sustainability Research Institute Groningen, ESRIG

Nijenborgh 6
9747 AG Groningen
T: 050 - 363 4760
W: www.rug.nl/research/esrig

ACKNOWLEDGEMENTS

First of all, I would like to thank dr. Ulrike Dusek for her supervision and valuable guidance throughout my thesis project. Secondly, I would like to show my appreciation to the Ph.D. Katrin Zenker and Ph.D. Yao Peng for their helpful teaching and friendly assistance in the lab. Furthermore, I want to thank Romke Tjoelker for teaching me filter and oven handling and helping me with any small problem I encountered in the lab and Henk Jansen for measuring ^{13}C signatures and carbon contents of several biomass material samples.

Finally I would like to thank Roland Vernooij and Patrik Winiger for their wonderful support to organize the test fires in the fire lab of Free University of Amsterdam and for collecting the aerosol samples from South Africa and Leipzig; and Chenxi Qiu for sharing the ^{13}C data of CO and CO_2 samples, measured in the laboratory of Utrecht University.

Contents

SUMMARY

Biomass burning results in emissions of greenhouse gases and aerosols to the atmosphere. The isotopic characterization of aerosols produced from combustion of vegetation may allow a better understanding of the source contribution from biomass fuels. In this research aerosol samples are collected, measured and analyzed from a series of laboratory experiments, where C_3 and C_4 plants (corn and willow wood), or C_3-C_4 plant mixtures are burned. The laboratory results are used to interpret the results of field studies, where smoke samples are collected in African savannah fires, where a mixture of C_4 (mainly grasses) and C_3 vegetation (bushes trees and leaves) is burned.

Results from the laboratory studies indicate that organic carbon (OC) from combustion of willow or corn shows $\delta^{13}C$ values comparable to the burned plant material. For combustion of willow, the $\delta^{13}C$ values in OC tend to be slightly higher (3.74% on average) than in the wood fuel, depending on combustion conditions. For combustion of corn, $\delta^{13}C$ values of OC tend to be slightly lower (2.44% on average) than in the fuel. For mixtures of willow and corn the relationship between $\delta^{13}C$ values in OC and the fuel mixture is slightly non-linear: For a 50-50% willow and corn mixture the $\delta^{13}C$ value in OC is around -19‰, closer to the value of corn than willow. Results of OC collected from the field studies show $\delta^{13}C$ values in the range of -22‰ to -25‰, which indicates more contribution from C_3 biomass fuels (approximately 68.27% from C_3 plants and 31.72% from C_4 plants on average) to the combustion than from C_4 biomass fuels (approximately 68.27% from C_3 plants and 31.72% from C_4 plants on average).

OC/EC ratio of the samples from corn burning is much higher than that from willow or wood chips burning. Depending upon combustion condition, combustion duration, moisture, OC/EC ratio varies in a quite large range: from 4.7 to 37.7 for samples from willow/ wood burning and from 44.7 to 112.4 for samples from corn burning. The proportion of corn and willow in biomass mixtures burnt shows a linear relation with OC/EC ratio. The light attenuation coefficients of the filter samples from different lab experiments and field experiments generally show linear relation with elemental carbon (EC) concentrations on the filter sample, as expected since higher EC is responsible for more attenuation.

1. INTRODUCTION

Biomass burning is a significant air pollution source, with global, regional and local impacts on air quality, public health and climate (Chen, et al. 2017). Biomass burning emissions include aerosols and gas-phase emissions from large-scale wildfires, prescribed fires, agricultural fires, charcoal production, and burning of biofuel for domestic heating and cooking purposes. By far the largest contributor (44%) to carbon emissions were fires in savannas and grasslands, with another 16% emitted from woodland fires (Werf, et al. 2010). Aerosol emitted by biomass burning can alter the radiative balance of the atmosphere through direct (scattering and absorption of light) and indirect (perturbation of cloud properties and atmospheric dynamics) processes, degrade urban and regional air quality, and harm human health. Africa is the single largest continental source of biomass burning emissions and it is estimated that open burning in Africa accounts for more than 50% of the total global biomass burning emissions during any typical year (Roberts, W. and Lagoudakis 2009), (Williams, et al. 2012).

In this research, biomass burning experiments were performed in the fire lab of Free University of Amsterdam and in a field campaign in South Africa with the goal to characterize CO_2 and CO emissions as well aerosol emissions. The research has been conducted in a collaboration project including the Free University of Amsterdam, Utrecht University, TNO and the University of Groningen where University of Groningen was responsible for the aerosol part. Aerosol filter samples collected from these lab and field experiments were analyzed for total carbon (TC), $\delta^{13}C$ value, OC/EC ratio and light absorption coefficients.

1.1 Carbonaceous aerosols

Atmospheric aerosols consisting of liquid or solid particles suspended in the air play an important role in many chemical processes occurring in the atmosphere (Mašalaitė, Garbaras and Remeikis 2012). Carbonaceous particles (aerosols) consist of two major components: organic carbon (OC) and graphite-like black carbon (BC) or elemental carbon (EC) (Seinfeld and Pandis 1998). Particulate organic matter (OC) can be either directly emitted from non-fossil and fossil sources (primary OC) or formed in the atmosphere via atmospheric oxidation of volatile organic compounds (secondary OC). Elemental carbon (EC) is only produced in incomplete combustion process of fossil fuels (e.g., coal, gasoline, and diesel) and biomass (e.g., wood, crop residues, and grass) and is therefore solely primary (Ni, et al. 2018). Black carbon (BC) is a useful qualitative description when referring to highly refractory, light-absorbing carbonaceous substances in atmospheric aerosol; however, for quantitative applications the term requires clarification of the underlying determination (Petzold, et al. 2013).

Traditionally the total carbon (TC) content of air particulate matter is defined as the sum of all carbon contained in the particles, except in the form of inorganic carbonates. TC is usually determined by thermo-chemical oxidation and evolved gas analysis (CO_2 detection) and divided into an organic carbon (OC) fraction and a black carbon (BC) or elemental carbon (EC) fraction. Measurements of BC and EC are generally based on optical and thermo-chemical techniques, and OC is operationally defined as the difference between TC and BC or EC (TC = BC + OC or TC = EC + OC) (Poschl 2005).

However, the definitions of EC and OC depend on the measurement techniques. EC is thermally stable in an inert atmosphere to high temperatures near 4000K and can only be gasified by oxidation starting at temperatures above 340°C. It is assumed to be inert and nonvolatile under atmospheric conditions and insoluble in any solvent (Petzold, et al. 2013). On the other hand, organic carbon can be volatilized at comparatively low temperature in absence of oxygen and at around 600°C OC is almost fully vaporized. During this volatilization process in absence of oxygen, a portion of OC turns into EC through charring. This process is normally called pyrolysis.

1.2 Biomass burning emissions

Practical uses of biomass burning include the clearing of forests and savannas for agricultural or grazing purposes, the shifting of crops produced in a location in order to replenish nutrients, the control of insects or other pests, and the domestic use of biomass matter for cooking and heating. Combustion of biomass results in atmospheric emissions of greenhouse gases and chemically active species in quantities that almost equal those produced by fossil fuel combustion (Ballentine, Macko and Turekian 1998), (D. C. Ballentine, et al. 1996). Biomass burning is the largest source of primary fine fraction (particles with a size upto 2.5 µm, $PM_{2.5}$) carbonaceous particles and the second largest source of trace gases in the global atmosphere (Bond, et al. 2004). Combustion of the individual fuel elements proceeds through a sequence of stages (ignition, flaming plus glowing plus pyrolysis, glowing plus pyrolysis (smoldering), glowing, and extinction), each with different chemical processes that result in different emissions. The quantity and type of emissions of trace gases as well as carbonaceous aerosols (OC and EC) from a biomass fire are determined not only by the type and composition of the fuel but also by the physical and chemical processes during combustion (Andreae and Merlet 2001)(Andrea). Therefore biomass burning emissions highly depend on the moisture content of the fuel, ambient temperature, humidity and local wind speed etc. (Seinfeld and Pandis 1998).

1.3 C_3-C_4 plants and Stable isotope ^{13}C

Stable carbon isotopes have been used for several decades to investigate sources of organic aerosol and its chemical processing (Dusek, et al. 2013). Atmospheric carbon dioxide contains approximately 1.1% of the non-radioactive isotope ^{13}C and 98.9% of ^{12}C. During photosynthesis, plants discriminate against ^{13}C because of small differences in chemical and physical properties imparted by the difference in mass. This discrimination can be used to assign plants to various photosynthetic groups. The isotope fractionation also reflects limitations on photosynthetic efficiency imposed by the various diffusional and chemical components of CO_2 uptake. Photorespiration is a wasteful pathway that occurs when the Calvin cycle enzyme rubisco acts on oxygen rather than carbon dioxide. Among higher plants, C_3 species have high levels of photorespiration, which limit the rate of net carbon dioxide assimilation. C_4 plants have evolved a mechanism that conserves water and overcomes photorespiration in dry climates (Monson, Edwards and Ku 1984). This important physiological division between the C_3 vs the C_4 pathway of carbon fixation during photosynthesis is also the reason for different isotopic fractionation in the initial fixation of CO_2 in the two pathways, therefore the ^{13}C : ^{12}C ratios also differ, with C_3 plants depleted in ^{13}C relative to C_4 plants (Hobbie and Werner 2004). C_4 plants typically have carbon isotopic signatures ranging from -17‰ to -9‰, whereas isotopic signatures for C_3 plants range from -32‰ to -20‰ (Ballentine, Macko and Turekian 1998).

1.4 Optical absorption

Light absorption by aerosols contributes to solar radiative forcing through absorption of solar radiation and heating of the absorbing aerosol layer. Besides the direct radiative effect, the heating can evaporate clouds and change the atmospheric dynamics. Aerosol light absorption in the atmosphere is dominated by black carbon (BC) (Moosmuuller, Chakrabarty and Arnott 2009).

Mainly due to the presence of black carbon (BC), ambient particulate material appears black when collected on a filter. Therefore, BC is defined as the fraction of carbonaceous aerosol absorbing light over a broad region of the visible spectrum and is measured by determining the attenuation of light transmitted through the sample (Weingartner, et al. 2003). Black carbon is a qualitative description when referring to light absorbing carbonaceous substances in atmospheric aerosol which is related to some measurable properties. The most commonly measured properties are elemental carbon (EC), a

mass metric, and the absorption coefficient, determined by light absorption (Ammerlaan, et al. 2017). The absorption coeffcient (b_{abs}) is defined with Beer–Lambert's law:

$$I = I_0 e^{-b_{abs}x} \quad (1)$$

where I_0 is the initial intensity of the beam, I(x) is its intensity after traversing a path length x. The absorption coefficient is commonly converted into a mass metric by application of a mass specific absorption cross section (MAC), referred to as mass absorption efficiency (MAE) which is the light abosrption coefficient of aerosol divided by EC.

1.5 Research aim and research questions

The main objective of this research is to analyze and characterize aerosol emissions from biomass burning of different C_3 and C_4 plants in the field campaigns in South Africa with help of the insight from a controlled biomass burning in the fire lab of Free University, Amsterdam.

Two sets of samples are collected and measured: one from controlled biomass burning in the laboratory environment and the other from infield biomass burning in South Africa. Therefore, two sets of research questions can be formulated which are given below:

a. Lab Experiment:
    1. What is the $\delta\ ^{13}C$ value of organic carbon of aerosol samples collected in the smoke of biomass burning and how does it compare to the actual ^{13}C signature of the biomass materials burnt?
    2. What is the impact of different mixtures of biomass materials (C_3 and C_4 plants) and different combustion conditions on the $\delta^{13}C$ of OC?
    3. What is the OC/EC ratio of the sampled aerosols?
    4. What are the light absorption properties of the collected aerosol? How can this be related to OC/EC ratio and the conditions of biomass burning (eg- ratio of biomass materials, burning efficiency etc.)?
b. Field Campaign:
    1. What is the $\delta^{13}C$ value of OC from aerosol samples collected in the smoke of controlled savanna fires in South Africa?
    2. How do different biomass materials (C_3 and C_4 plants) contribute to the $\delta^{13}C$ of OC?
    3. What is the OC/EC ratio and light absorption properties of the aerosol, and how they are related?

2. METHODS

In this research we used a thermo-optical method to analyze concentrations of OC and EC on the filter samples, isotope ratio mass spectrometry (IRMS) to measure $^{13}C/^{12}C$ ratios of OC, as well as analysis of optical properties of the black carbon aerosols. Filter samples were collected in two phases:

1. Fire experiments in the Laboratory: Biomass burning took place in the laboratory to collect the aerosol samples. Then samples were measured and analyzed in RUG laboratory.
2. Field experiments in South Africa: Biomass burning took place in several plots of South Africa. Aerosol samples were collected in the filters and then measured and analyzed in RUG laboratory.

2.1 Sample collection

2.1.1 Filter preparation

In order prevent any type of contamination, filter handling is very important. Aerosol samples are collected on 37mm quartz fiber filters (Tissuquartz 2500QAT-UP, Merck). Before using these filters to collect the aerosols, they are pre-heated to 650°C for more than 3 hours. These pre-cleaned (or pre-heated) filters are wrapped in aluminum foil which are already pre-heated to 550°C for more than 2 hours. Then the filters along with the aluminum foil, are kept in sealed polyethylene bags until being used for collecting the aerosols or measuring. Instruments like punchers, tweezers are always cleaned with acetone and ethanol before having contact with the filter.

2.1.2 Biomass burning & aerosol collection

For a good burn, biomass materials should be dried well. Also there should be enough air circulation. In the laboratory experiment, biomass materials are burnt on a metal tray inside a glass chamber as shown in the figure: 2-1. The smoke is drawn into a chimney where the filter holder along with the pre-cleaned quartz fiber filter in it is placed within a safe distance (around 100-120 cm) above the flame. The filter holder is connected to a flow controlled pump through a long poly-urethane tube. Just before the starting of biomass burning, the pump is turned on so that the filter in the holder can collect the aerosols passing through it. With the help of a mass flow controler in the pump a constant flow of 3L/min is maintained. With an $PM_{2.5}$ inertial impactor (Personal Modular Impactor, SKC) produces a homogeneous deposit on the filter, thus size segregated aerosol samples upto 2.5 µm are collected. With this setup aerosol sample is collected for 5 minutes to 30 minutes depending upon the amount of fuel, burning condition (flaming or smoldering) etc. After the fire is stopped, filter sample is taken out of the holder, wrapped in the aluminum foil and kept in the air-tight bag until measurement.

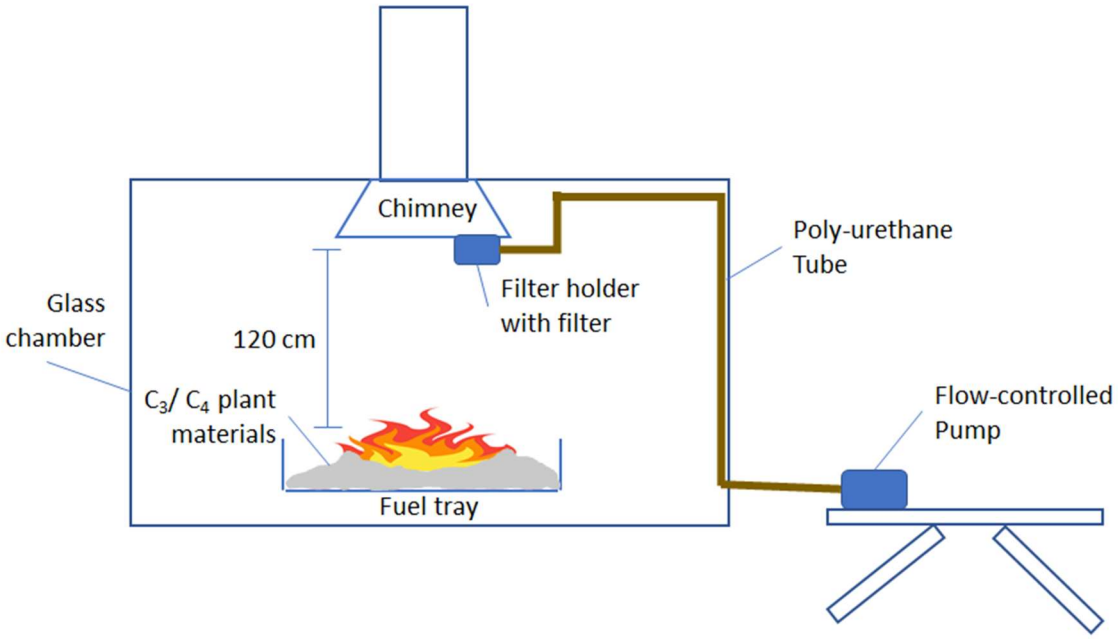

Figure 2-1 Schematic diagram of the experimental setup for biomass burning in the laboratory experiment.

In the field experiment, a similar experimental setup is used to collect the aerosol sample, except the biomass burning that takes place in an open environment instead of a glass chamber and the filter holder that is placed at the top of a telecospic overhead mast as shown in the figure:2-2. The mast can be extended to a maximum height of 13 meters and an effective height of 5 to 12 meters is used based on the plot area, plants height and the wind speed (for wider area, taller C_3 plants and lower wind speed, the mast height is kept larger so that the filter can collect a well mixture of aerosol products from a heigher position). For stability, an auger with the same diameter of the mast is used to create a 0.5m hole on the ground and the top of the mast is fixated using guide wire on 4 sides. A box with measurement equipment is kept on the leeward side of the mast. Both the mast and the box are protected using insulating rockwool. The mast is set up at a position in the plot with continuous representative fuel in the upwind direction. A platform mounted to the top of the mast holds a filter holder and inlet of a long poly-urethane tube. The long poly-urethane connects the filter holder to a flow-controlled pump that creates a constant 3 L/min flow at which inertial impactor (Personal Modular Impactor, SKC) installed inside the filter holder provides a cutoff of roughly 2.5µm.

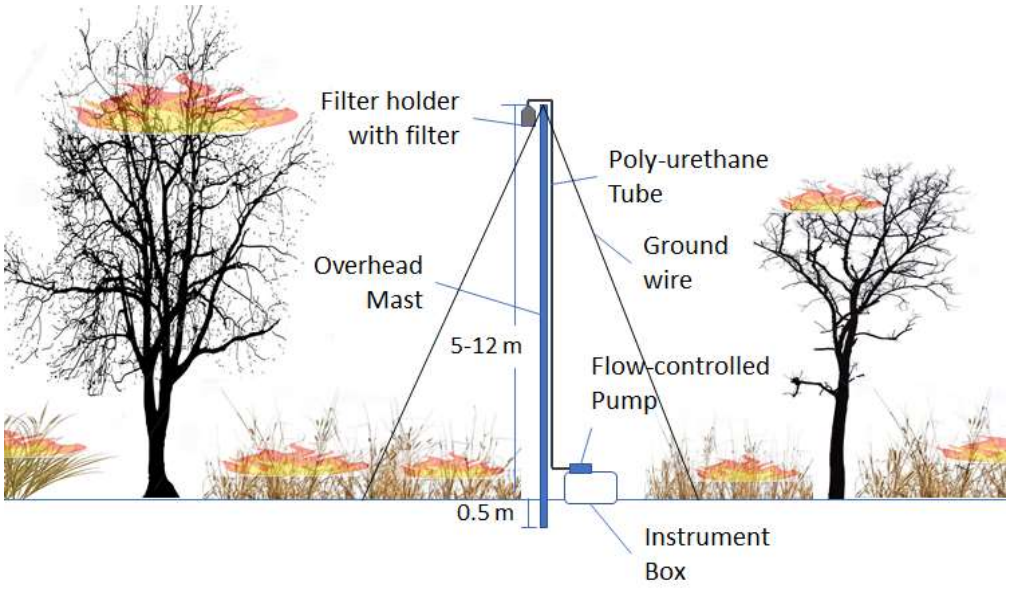

Figure 2-2 Schematic diagram of the experimental setup for biomass burning in the open field

During the biomass burning in both laboratory experiments and field experiments, CO_2 and CH_4 were measured using a cavity-ringdown spectrometer (Los Gatos Research, Micro-portable Greenhouse Gas Analyzer), CO and N_2O were measured using an Aeris Technologies Pico series N_2O and CO analyzer by Free University team. Also during the biomass burning in some of the laboratory experiments, the air sample passing through the poly-urethane tube was collected in a Tedlar® sample bag and then reallocated to a ultra-cleaned and vacuumed (10^{-5} mbar) glass flask (1L) in order to measure $\delta^{13}C$ of CO_2 and CO by Utrecht University team. Data of measured CO and CO_2 from glass chamber and those from the ambient during the biomass burning in laboratory experiments was used in this research to calculate the modified combustion efficiency (MCE). For field experiments, data of measured CO and CO_2 before and during biomass burning was used.

2.1.3 Sample transport and preservation

After collecting the aerosols, filter samples are preserved at -20°C in a freezer until analysis. During transportation they are cooled with ice bags.

2.2 Measurement of total carbon

A small piece of each filter sample is used to measure the total carbon content in the filter. This information allows to select an appropriate punch area for the ^{13}C measurement. Depending upon the TC content and filter size, one or two 1.5cm^2 pieces of the filter are used for ^{13}C measurement, even if the TC content of the filter is very low (almost blank), then the filter cannot be used for the ^{13}C measurement. Therefore, measurement of total carbon is performed before going for the ^{13}C measurement. For the measurement of total carbon, a thermal-optical carbon analyzer (Sunset Laboratory, Inc.) is used with the protocol: total_carbon.par.

2.2.1 Experimental Setup

Fig-2.2 shows the Sunset thermal-optical carbon analyzer along with the computer system where the operating SW is installed, and data is stored. The Sunset instrument is intended for measuring the amount of organic carbon (within the range from 0.01 to 600 µg/cm^2) and elemental carbon (within the range from 0.01 to 20 µg/cm^2) on filters.

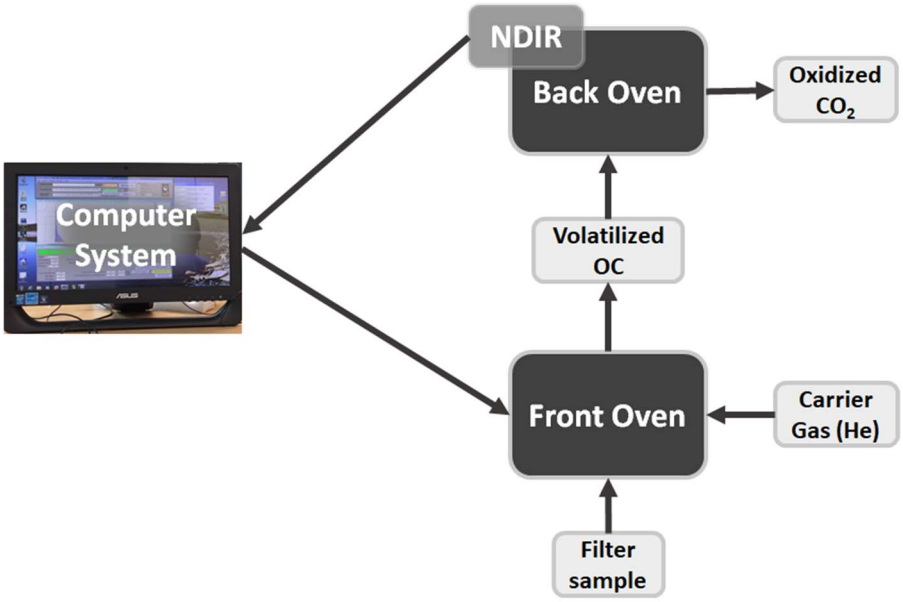

Figure 2-3. Thermal-optical carbon analyzer (Sunset Laboratory, Inc.)

The Sunset analyzer consists of two quartz ovens: a front oven with an inlet and a back oven with an outlet. With a clamp front oven inlet is connected to the gas supply tube, through which either He or a He/O_2 mixture can be supplied as carrier gas. A sample spoon made of quartz glass is placed inside front oven underneath a laser beam perpendicular to the oven. On this sample spoon one or more piece(s) cut from the quartz filter sample is/ are placed. Once the oven is purged with pure helium or He/ O_2 mixture, the oven temperature is increased in one or several defined temperature steps. In pure helium condition, organic compounds in the sample are thermally desorbed and are transported into the oxidizing back oven by the He carrier gas. As the evaporated organic molecules flow through the back oven they are quantitatively converted to CO_2 gas. The CO_2 is quantified by a self a self-contained non-dispersive infrared (NDIR) detector. In He/O_2 condition at temperatures of 850°C, any carbon (EC, OC or total carbon) is combusted from the filter and detected in the same manner as the organic carbon. Temperature ramp, gas flow, time spans etc. can be adjusted using different protocols which can be standard or user defined for various purposes.

2.2.2 Description of the protocol for TC measurement

A small piece from the filter sample is cut with 4- or 6-mm puncher and placed into the front oven. With the protocol total_carbon.par, the sample in the front oven is heated with helium/ oxygen mixture in a single temperature step up to 850°C for 330s and all the carbonaceous material is oxidized to CO_2 which is then measured to get the amount of TC.

2.3 OC/EC measurement

For the measurement of OC/EC ratio, the thermal-optical carbon analyzer of Sunset Laboratory, Inc. is used along with the protocol EUSAAR2.

2.3.1 Experimental setup and protocol description

The experimental setup for the measurement of OC/EC ratio is same as the measurement of total carbon, only the protocol used is different. The EUSAAR2 protocol is used to analyze different carbonaceous aerosol fractions (OC/EC fraction) on a Sunset analyzer (Cavalli, et al. 2010). First, the filter piece of 1.5 cm^2 is taken and put into the front oven. With EUSAAR2 protocol different OC fractions are measured in an inert atmosphere (He) at 200°C for 120s, at 300°C for 150s, at 450°C for

180s and at 650°C for 180s. Then EC fractions are analyzed in an oxidizing atmosphere (He/O_2) at 500°C for 120s, at 550°C for 120s, at 700° C for 70s, and at 850°C for 80s.

Table 2-1. Temperature and duration(s) of EUSAAR2 protocol

Step	Carrier gas	Temp (°C)	Duration (s)
OC1	pure He	200	120
OC2	pure He	300	150
OC3	pure He	450	180
OC4	pure He	650	180
EC1	2%O_2/98%He	500	120
EC2	2%O_2/98%He	550	120
EC3	2%O_2/98%He	700	70
EC4	2%O_2/98%He	850	80
Detector		NDIR	
Pyrolysis correction		Transmittance	

2.3.2 Pyrolytic Carbon (PC) correction

When OC is desorbed during the first four temperature steps in He, some part of OC chars and turns into EC. Thus, the output from these OC and EC steps contain a bit more EC and less OC than their original values. To correct for this pyrolysis (thermal decomposition of organic carbon at elevated temperatures in an inert atmosphere), the optical properties of the sample are monitored with a laser beam. Since PC absorbs the laser light and OC does not, light transmission decrease while OC chars in the He. And when PC (and EC) are released from the filter in the He/O_2-mode, transmission and reflectance increase again. The point at which the transmission reach the pre-pyrolysis value is defined as the split point, which is used to discriminate OC and EC (Cavalli, et al. 2010) instead of using the EC1 temperature step (500^{o}C) point.

2.4 Measurement of $\delta^{13}C$ of OC

A thermogram system (thermal-desorption IRMS system) is used to analyze $\delta^{13}C$ in organic carbon (OC) released from aerosol filter samples in helium during different temperature steps. One out of two temperature protocols for the sunset oven can be used: ZWO_1step330_V4 for single step and ZWoptima_3steps_V5 for 3 temperature steps.

2.4.1 Experimental Setup

Figure:2-4 shows the thermogram system which comprises a Sunset OC/EC analyzer and an isotope ratio mass spectrometer (IRMS) model Optima from Fision instruments. Both of them are connected via a custom-made interface for CO_2 collection and purification, which comprises a series of instruments such as a dryer, a 6-port switching valve, two liquid nitrogen traps, and a gas chromatoghy (GC) column. The system setup is described in (Dusek, et al. 2013) and (Zenker, et al. 2019). An overview of the working principle has been discussed here.

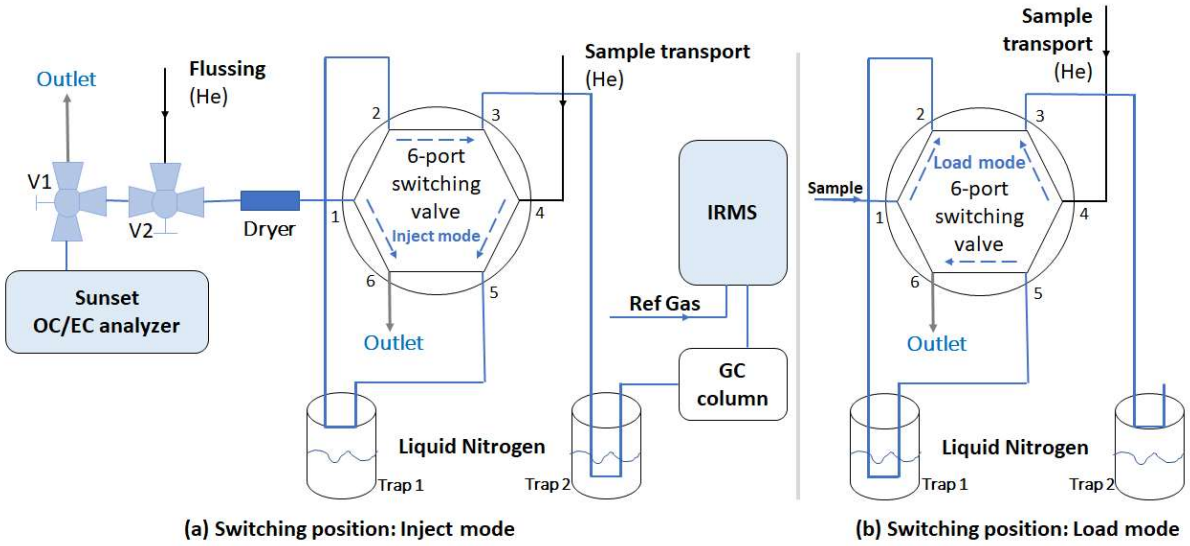

Figure 2-4. The experimental setup of the $\delta^{13}C$-thermogram system. (a) the 6-port switching valve at inject mode, (b) the 6-port switching valve at load mode.

The filter sample (one piece with the punch area of 1 cm^2 or 1.5 cm^2 or two pieces with 1.5 cm^2 each, depending upon the TC content on the filter) is placed in the front-oven of the Sunset analyzer using a movable quartz glass spoon (a filter holder). Temperature of the front oven can be changed according to the protocol settings and organic carbon (OC) from the sample is desorbed in different temperature steps. All the desorption products are oxidized by a catalyst (manganese dioxide, MnO_2) in the back-oven and exit the Sunset analyzer under a constant stream of helium to enter the dryer filled with hygroscopic phosphorus pentoxide (P_2O_5). Then the dehydrated sample reaches the port 1 of the six-port-valve, which can switch between two different modes: load mode and inject mode. During the desorption process the six-port-valve is at the 'load' mode as shown in the figure:2-4 (b) and the desorption products are flushed through port 1 to port 2 and then trough the trap 1, which is submerged in the liquid nitrogen. All desorption products (mainly CO_2, but also likely NO_x and SO_2) with sufficiently low vapor pressure are condensed and collected in trap 1. The rest of the gases with lower boiling point than N_2 (-196°C) are flushed out through port 5 and outlet port 6 and exit the system through the vent. After the complete collection of the desorption products, the six-port-valve is switched to the 'inject' 'mode where the gas flow from the Sunset analyzer passes through port 1 to port 6 and is directly vented to the lab. Trap 1 comes out of the liquid nitrogen and is warmed up to room temperature. A separate helium stream (sample transport) is flushed from the opposite direction through port 4 to port 5, trap 1, port 2 to port 3 and trap 2. The sample is purged from trap 1 to the focus trap 2 where it is condensed and collected again, since the trap 2 in this mode is submerged in the liquid nitrogen. Finally trap-2 comes out of the liquid N_2 to warm up the sample and sample gases eneter the gas chromtography (GC) column where other gases like N_2O are elimintaed. Thus the pure CO_2 enters into the IRMS, where CO_2 molecules are ionized, ionized masses are separated based on charge to mass ratios (m/z) and finally they are detected in the m-44, m-45 & m-46 Faraday cup detectors and later converted to a digital output. The reference gas is added separately to the helium flow and directly enters the IRMS. The whole setup, mainly the lifting and lowering of the traps, the switching of the six-port-valve and the IRMS, is controlled by a programmable logic controller (PLC).

2.4.1.1 Isotope Ratio Mass Spectrometer (IRMS)

Mass spectrometry is an analytic method to determine the abundance ratios of different components of an unknown mixture of different isotopes of an element or isotopologues of molecules, either in solid state, fluid or gaseous. The basic principle of mass spectrometry is to generate ions from either inorganic or organic compounds by any suitable method, to separate these ions by their mass-to-charge ratio (m/z) and to detect them qualitatively and quantitatively by their respective m/z and abundance. [Gross, 2017]. An isotope ratio mass spectrometer (IRMS) consists of three major parts: (a) ion source that creates gas phase ions, (b) mass analyzer that takes ionized masses and separates them based on charge to mass ratios (m/z) using a magnetic field, and (c) detector that converts the energy of incoming particles into a current signal that is registered by the electronic devices and transferred to the computer of the acquisition system of the mass spectrometer. The Faraday cup detector is very much in use today. Since the mass analyzer and the detector (and many of the ion sources) require low pressure for operation the instrument also needs a pumping system. Moreover, a computer-based system is required to record the signal registered by the detector and to process much of the acquired data. A schematic of IRMS is depicted in the figure:2-5.

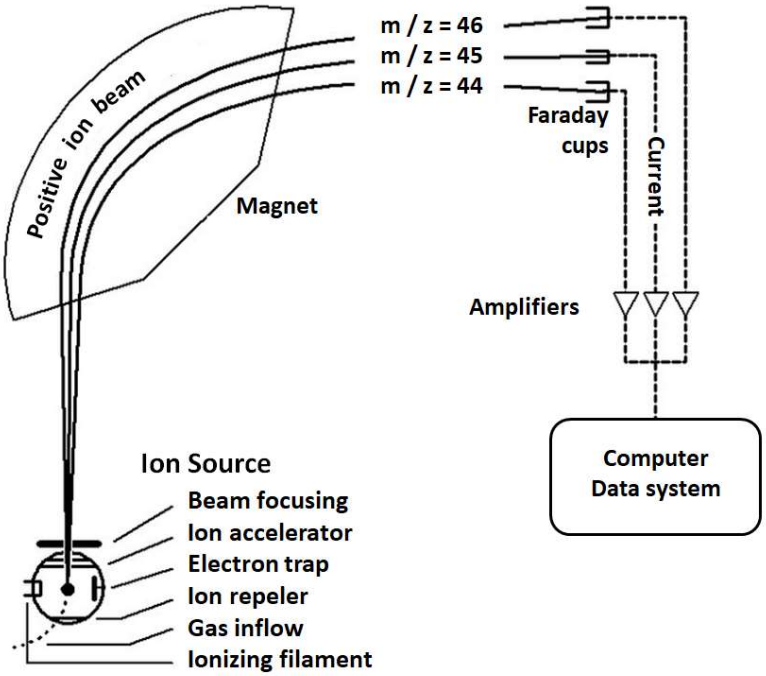

Figure 2-5. The schematic diagram of isotopic ratio mass spectrometer (IRMS)

2.4.2 Description of protocols used in Sunset

In the Sunset carbon analyzer, OC is volatilized at three temperature steps (for ZWoptima_3steps_V5) or at one temperature step (for ZWO_1step330_V4) in pure Helium and then oxidized in the back oven with a catalyst to form CO_2. Initailly front oven is flushed with pure He at 30°C for 31s (flushing step OC1). Then it is heated to three temperature steps of 200°C, 350°C and 650°C for ZWoptima_3steps_V5 protocol and single temperature step is 650°C, each step sustains for 330s and pure He gas is flushed. After all the OC is desorbed in front oven and oxidized in the back oven, the filter is heated to 850°C for 240s with helium and oxygen mixture which oxidizes the rest EC contents on the filter sample, but EC is currently not measured in the IRMS. This step removes of all remaining carbon from the filter sample and avoids a carry-over of contamination to the next measurement.

Table 2-2 Temperature and duration(s) of ZWO_1step330 and ZWOptima_3steps protocols

		ZWoptima_3steps.V5		ZWO_1step330.V4	
Step	**Carrier gas**	**Temp (°C)**	**Duration (s)**	**Temp (°C)**	**Duration (s)**
OC1	pure He	30	31	30	31
OC2	pure He	200	330	650	330
OC3	pure He	350	330		
OC4	pure He	650	330		
EC1	2%O_2/98%He	850	240	850	240
EC2					
EC3					
EC4					
Detector		NDIR			
Pyrolysis correction		Transmittance			

2.4.3 $\delta^{13}C$ Calculation

The ^{13}C content of a sample is expressed in the delta notation as $\delta^{13}C$, which is defined as the relative deviation of the isotope ratio of the sample from that of the standard and is given in the below equation:

$$\delta_{S\to R} = \left(\frac{R_{Sample} - R_{Standard}}{R_{Standard}}\right).1000‰ = \left(\frac{R_{Sample}}{R_{Standard}} - 1\right).1000‰ \quad (2)$$

Where the isotope ratio can be found in the below equation:

$$^{13}R = \frac{[^{13}CO_2]}{[^{12}CO_2]} \quad (3)$$

The isotope ratios are reported with respect to the international primary standard Vienna Pee Dee Belemnite (VPDB).

2.4.3.1 Background correction

In the IRMS the ionized masses of CO_2 are separated based on the charge to mass ratios (m/z) and then detected in Faraday cups which gives the outputs in current (Amps) for mass-44, 45 and 46. The values from the peak integration (PI) for mass-44, 45 and 46 used in the calculation with a background correction. Before the sample and reference CO_2 entering the IRMS, everything is flushed by inert He gas and the background peak integration values are taken which represents any type of residues or contamination from previous samples. Background correction is given in below equations:

$$^{45}R = \frac{[^{45}PI_{Sample}] - [^{45}PI_{bgr}]}{[^{44}PI_{Sample}] - [^{44}PI_{bgr}]} \quad (4)$$

$$^{46}R = \frac{[^{46}PI_{Sample}] - [^{46}PI_{bgr}]}{[^{44}PI_{Sample}] - [^{44}PI_{bgr}]} \quad (5)$$

2.4.3.2 ^{17}O correction

$\delta^{13}C$ obtained from above isotope ratio ^{45}R is not exactly same as the desired $\delta\ ^{13}C$ value.

$$\delta^{13}C \approx \delta^{45}CO_2 = \frac{[^{45}R_{Sample}]}{[^{45}R_{Reference}]} - 1 \quad (6)$$

As mass-45 contains other isotope than ^{13}C, $\delta^{13}C$ from ^{45}R doesn't give exact value. Mass-45 contains $^{13}C^{16}O_2$ and $^{12}C^{16}O^{17}O$ (and mass-46 contains $^{12}C^{18}O^{16}O$, $^{13}C^{17}O^{16}O$ and $^{12}C^{17}O^{17}O$). Therefore, the isotope ratios of ^{45}R and ^{45}R can be defined as:

$$^{45}R = \frac{[^{13}C^{16}O_2] + [^{12}C^{16}O^{17}O]}{[^{12}C^{16}O_2]} \quad (7)$$

$$^{46}R = \frac{[^{12}C^{18}O^{16}O] + [^{13}C^{16}O^{17}O] + [^{12}C^{17}O^{17}O]}{[^{12}C^{16}O_2]} \quad (8)$$

As shown in the equation-7 of ^{45}R, it contains ^{17}O isotope. Therefore, $\delta^{13}C$ calculated from ^{45}R (ie, the ratio of the m/z 45 and m/z 44 ion currents) requires a correction for this the ^{17}O contribution to the m/z 45 ion beam. This correction is done through below three approximations (Craig 1957):

$$(\frac{^{18}R_{Sample}}{^{18}R_{Std}})^{\lambda} = \frac{^{17}R_{Sample}}{^{17}R_{Std}} \quad (9)$$

$$\frac{^{45}R_{Std}}{^{13}R_{Std}} = 1.0676 \quad (10)$$

$$\frac{^{17}R_{Std}}{^{13}R_{Std}} = 0.0338 \quad (11)$$

Above three equations- 9, 10 and 11, give a simple quantity equation for correcting measured isotopic differences using the m/z 44, 45, and 46 ion currents which is given below (Craig 1957):

$$\delta\ (^{13}C) \approx 1.0676 * \delta(^{45}CO_2) - 0.0338 * \delta(^{18}O) \quad (12)$$

The relation between isotopic ratio of ^{46}R, ^{17}R and ^{13}R is given in the below expression (Brand, Assonov and Coplen 2010):

$$^{46}R = {}^{2}{}^{18}R + 2\ {}^{17}R\ {}^{13}R + (^{17}R)^2 \quad (13)$$

Ignoring the terms $^{17}R.^{13}R$ and $(^{17}R)^2$ in the equation-13, it can be simplified as:

$$^{46}R \approx {}^{2}{}^{18}R \quad (14)$$

This gives:

$$\delta^{46} = \frac{^{46}R_{Sample}}{^{46}R_{Std}} - 1 \approx \frac{2\ ^{18}R_{Sample}}{2\ ^{18}R_{Std}} - 1 \approx \delta^{18}$$

$$\delta^{18}O \approx \delta^{46}CO_2 \quad (15)$$

Therefore from the equations- 12 and 15, the final simplified expression for ^{17}O correction is obtained as follows:

$$\delta\,(^{13}C) \approx 1.0676 * \delta(^{45}CO_2) - 0.0338 * \delta(^{46}CO_2) \quad (16)$$

2.4.3.3 $\delta^{13}C$ with respect to VPDB

The reference gas used in the laboratory experiment is not the VPDB standard gas. The $\delta^{13}C$ of this reference gas with respect to VPDB is 3.9‰ and can be given by below equation:

$$\delta_{R\to V} = \frac{R_{Reference}}{R_{VPDB}} - 1 \quad (17)$$

Finally, $\delta^{13}C$ of the sample with respect to VPDB is obtained according to below calculations:

$$\begin{aligned}\delta_{S\to V} &= \frac{R_{Sample}}{R_{VPDB}} - 1 \\ &= \frac{R_{Sample}}{R_{Reference}} * \frac{R_{Reference}}{R_{VPDB}} - 1 \\ &= (1 + \delta_{S\to R}) * (1 + \delta_{R\to V}) - 1 \\ &= 1 + \delta_{S\to R} + \delta_{R\to V} + \delta_{S\to R} * \delta_{R\to V} - 1\end{aligned}$$

$$\delta_{S\to V} = \delta_{S\to R} + \delta_{R\to V} + \delta_{S\to R} * \delta_{R\to V} \quad (18)$$

2.4.3.4 CAN-CAF Correction

$\delta^{13}C$ values of standard CAN and CAF solutions with known $\delta^{13}C$ values (-38.2‰ and 0.61 ‰ respectively) are measured using the same Sunset-IRMS setup. Actual $\delta^{13}C$ values of CAN and CAF solutions are plotted with respect to the measured ^{13}C values. Intercept (a) and slope (b) are determined.

With this slope and intercept, measured $\delta^{13}C$ values of the samples (with respect to VPDB) are corrected. If the measured $\delta^{13}C$ (with respect to VPDB) is x, then corrected value (y) will be:

$$y = a + bx \quad (19)$$

^{13}C of CAN and CAF are measured twice a day: in the morning before starting the measurements of samples and at the end of the day after completing the measurements of sample. Samples measured in the first half of the day are corrected with CAN/ CAF data of morning measurements and samples measure in the 2nd half are corrected with CAN/CAF data of evening measurements.

$\delta^{13}C$ value of a third standard- LVAL solution with a known $\delta^{13}C$ value (-24.03 ± 0.04 ‰) is also measured using the same Sunset-IRMS setup. Then with obtained slope and intercept, the measured $\delta^{13}C$ is corrected for this LVAL solution and it is checked with its original known value if they are close enough.

2.5 Optical Method

The optical attenuation of light (ATN) is defined as the attenuated fraction of light passing through a filter sample (transmittance measurement) and from Lambert-Beer law it can be given as below equation:

$$\mathrm{ATN} \approx ln\,(\frac{I_0}{\mathrm{I}}) \quad (20)$$

where I_0 is the intensity of the incident laser beam and I is the intensity of the light passing through the filter.

With the Sunset carbon analyzer, the attenuation cannot be determined directly, because the initial laser intensity I_0 is unknown. However, the difference in attenuation ΔATN between a dark filter sample and white filter, can be measured. It can be given as below equations:

$$\begin{aligned}\Delta\mathrm{ATN} &\cong ln\left(\frac{I_0}{I_{Td}}\right) - ln\left(\frac{\eta I_0}{I_{Tw}}\right)\\ &= ln\left(\frac{I_{Tw}}{I_{Td}}\right) - ln\left(\frac{\eta I_0}{I_0}\right)\\ &= ln\left(\frac{I_{Tw}}{I_{Td}}\right) - ln(\eta)\end{aligned}$$

where I_{Tw} is the intensity of the transmitted light passing through a white filter, I_{Td} is the intensity of the transmitted light through a dark filter and η the variation of the incident beam in time. η is assumed to be close to 1 during the analysis, so the second logarithm, ln(η), is negligible.

$$\Delta\mathrm{ATN} \approx ln\left(\frac{I_{Tw}}{I_{Td}}\right) \quad (21)$$

The attenuation coefficient $b_{ATN;Sunset}$ (with the units of m^{-1}) can be obtained from the measured difference in attenuation Δ ATN as per below equation:

$$b_{\mathrm{ATN;Sunset}} = \frac{A}{\mathrm{Q}}\frac{\Delta\mathrm{ATN}}{\Delta\mathrm{t}} \quad (22)$$

where A is the filter area (in m^2), Q is the volumetric flow rate (in m^3s^{-1}) and Δt is the sampling time (in s). Here, the total sampled volume V can be used as V ≡ QΔt (in m^3). Therefore, using equations-21 and 22:

$$b_{\mathrm{ATN;Sunset}} = \frac{A}{\mathrm{V}}\, ln\left(\frac{I_{Tw}}{I_{Td}}\right) \quad (23)$$

The measured attenuation coefficient differs from the absorption coefficient of the aerosols in air. This is caused by a multiple scattering enhancement and a loading effect, which is sometimes also referred to as 'shadowing effect' (Ammerlaan, et al. 2017). To correct for these artefacts, a correction function C.R(ΔATN) is introduced, where C parametrises the multiple scattering enhancement and R(ΔATN) parametrises the loading effect (Ammerlaan, et al. 2017). The absorption coefficient is then calculated by:

$$b_{\mathrm{abs}} = \frac{b_{\mathrm{ATN}}}{\mathrm{C.R}(\Delta\mathrm{ATN})} \quad (24)$$

In order to determine the correction factor or calibration factor C.R(ΔATN), calibration is done between a MAAP instrument and the Sunset analyzer. From the MAAP the absorption coefficient, $b_{abs;MAAP}$ is directly obtained during the bimass burning and from the Sunset analyzer attenuation coefficient $b_{ATN;Sunset}$ is obtained for the aerosol sample collected during same fire using the equation-23. With several measurements, the data points of $b_{abs;MAAP}$ and $b_{ATN;Sunset}$ will give a best fit of the line y = bx where y = $b_{ATN;Sunset}$ and x = $b_{abs;MAAP}$. The slope b will be then the required correction factor or calibration factor C.R(ΔATN).

After such calibration between the MAAP and Sunset instruments, the absorption coefficient of aerosols can be calculated from the attenuation coefficient measured by the Sunset with the help of calibration factor:

$$b_{\mathrm{abs;Sunset}} = \frac{b_{\mathrm{ATN;Sunset}}}{\mathrm{C.R}(\Delta\ \mathrm{ATN})} \quad (25)$$

Finally using $b_{abs;Sunset}$ and the elemental carbon concentration from these instruments (EC in μg m^{-3}), the mass absorption efficiency of EC (MAE) for each sample can be calculated as:

$$MAE = \frac{b_{\mathrm{abs;Sunset}}}{\mathrm{EC}} \quad (26)$$

3. RESULTS

3.1 Total carbon vs OC peaks

All the filter samples are first measured for total carbon content to check if they contain enough carbon content to proceed for further steps. A small piece of 6mm or 4mm diameter punches (0.13 cm^2 or 0.28cm^2) is taken from the filter sample to measure. Since such a tiny piece is taken for the measurement, sometimes total carbon measurement deviated from the original value, especially for the filter samples with low carbon concentrations. To check the consistency of total carbon measurement scatter plot of TC vs total OC concentrations are shown in fig. 3-1 (a) for samples from lab experiments and fig. 3-1 (b) for field experiment samples. OC peaks here is the sum of OC peaks of three temperature steps obtained during the δ ^{13}C measurements.

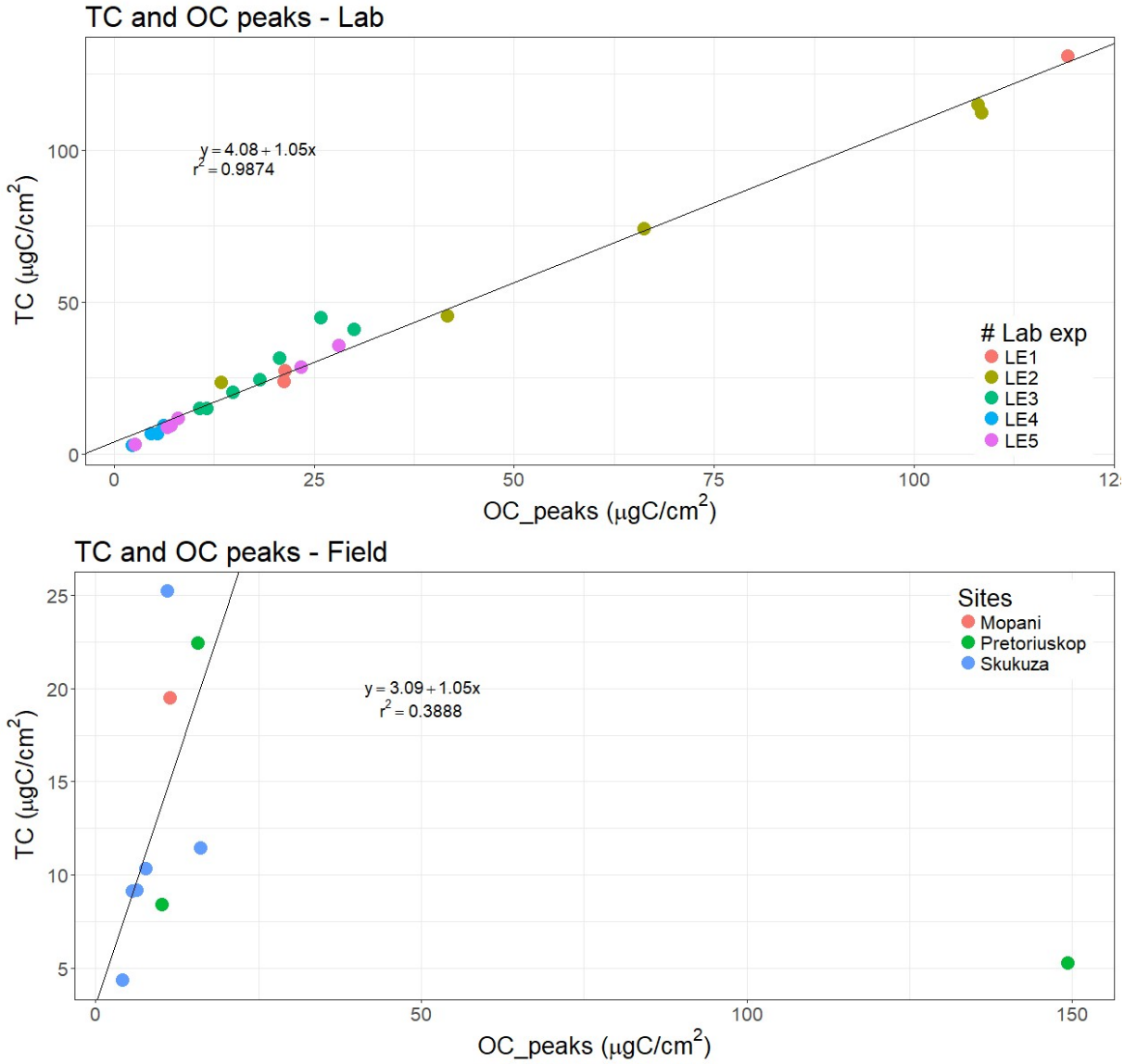

Figure 3-1. TC vs OC concentrations for the samples from a) 5 LAB experiments b) Field experiments of three sites in South Africa

From the above graphs it can be seen that TC and OC concentrations are linearly related for the lab experiment samples, with TC concentrations always greater than OC peaks as expected. On the other hand, TC and OC peak for field experiment samples are more scattered and for a few samples OC peak is larger than TC which definitely indicates the wrong measurement. Since most of samples from field experiment have very low carbon concentrations, the total carbon measured on a tiny piece of small punch area (0.28 cm^2) is on the order of the detection limit of the instrument. This is the main reason of not getting a linear relationship between TC and OC peak. There are also several filters from the field campaign for which the carbon concentration barely exceeds the one from the blank filter and these cannot be measured for $\delta^{13}C$ value.

3.2 OC/ EC Ratio

OC/EC ratios of the samples from willow, wood chips and corn burning in the lab experiments are listed in the table 3-5 and also shown in the fig:3-8 (a). OC/EC ratio of the samples from same biomass burning is impacted by the duration of biomass burning, moisture, combustion condition etc. But in general, OC/EC ratio of the samples from corn burning (44.7 to 112.4). is much higher than that from willow or wood chips burning(4.7 to 37.7) From the table, it can be found that if same biomass in the same experiment is burned, then with long duration of fire tends to cause higher OC/EC ratio (with few outliers). In lab experiment 4, sample from the burning of wood chips with added moisture (LAB4_WO6) has much higher OC/EC ratio than samples from the burning of dry wood chips (LAB4_WO2 and LAB4_WO6).

Table 3-1. OC/EC ratio of samples from willow, wood chips and corn burning. In the filter names, LAB denote the laboratory experiments 1, 2, ... 5.

Filtername	Biomass	Duration	OC (ug/ m^3)	EC (ug/ m^3)	TC (ug/ m^3)	OC/EC ratio
LAB1_WI3	Willow	600	218.95	5.99	224.94	36.56
LAB1_WI4	Willow	900	4259.24	113.11	4372.35	37.66
LAB2_C2	Corn	300	942.46	14.54	956.99	64.82
LAB2_C3	Corn	390	4996.06	50.69	5046.75	98.56
LAB2_C4	Corn	525	6322.24	78.29	6400.53	80.75
LAB2_C5	Corn	858	4010.25	35.68	4045.93	112.39
LAB3_C1	Corn	1320	304.95	6.82	311.76	44.74
LAB3_WI1	Willow	1805	574.95	121.93	696.88	4.72
LAB4_WO2	Wood chips	300	534.35	83.27	617.62	6.42
LAB4_WO4	Wood chips	600	370.78	45.41	416.19	8.17
LAB4_WO6	Wood chips (wet)	600	144.07	5.11	149.18	28.21
LAB5_C1	Corn	720	1038.23	11.64	1049.87	89.23

Fig. 3-9 (b) shows the relation between the C/EC ratio and the proportion of corn and willow in biomass mixtures burnt in the 3rd lab experiment. The Aerosol sample from burning of pure willow (ie, 0% corn) has an OC/EC ratio of 4.72. While increasing the percentage of corn in the biomass mixtures, the OC/EC ratio of the aerosol samples shows a clear increasing trend, with the sample from 100% corn burning having an OC/EC ratio of 44.74. Since corn contributes much more than willow to the organic carbon (OC), it has higher contribution in $\delta^{13}C$ as well, ie with 50%-50% mixture, $\delta^{13}C$ value is closer to the $\delta^{13}C$ of 100% corn as found in section 3-2-2.

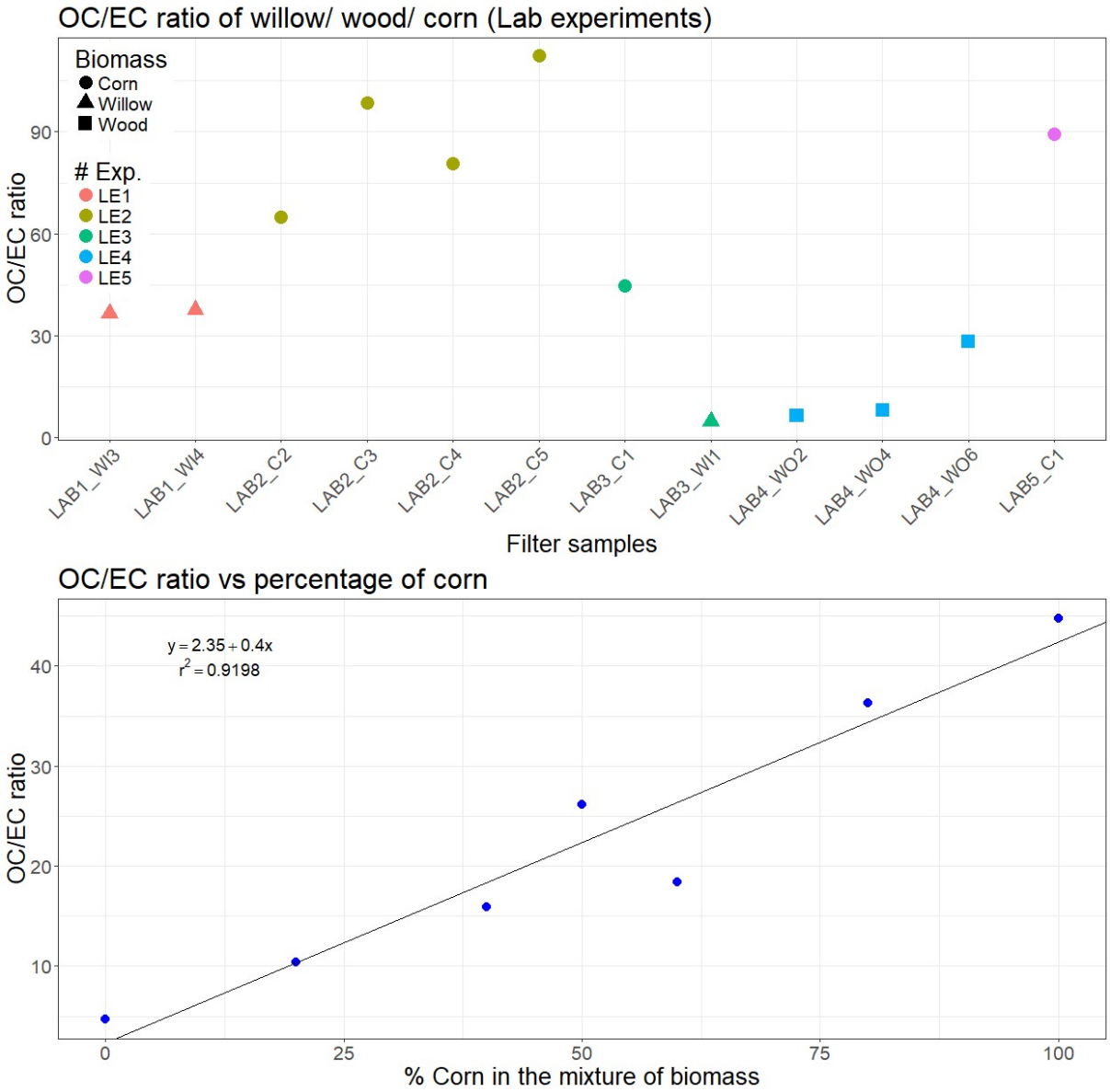

Figure 3-2. OC/EC ratio of lab experiment samples. a) OC/EC ratio of willow, wood and corn. b) OC/EC ratio vs percentage of corn in the mixture of biomass burnt (lab experiment:3)

In fig. 3-10, OC/EC ratio of the samples from field campaigns is shown. The samples from the biomass burning in the field campaigns have the OC/EC ratio in the range of 6.3 to 18.5. Since the OC/EC ratio of the aerosols formed by burning of C_3 and C_4 plants individually in the plots of field experiments, is unknown, it is not possible to find which plants have higher contribution in these samples.

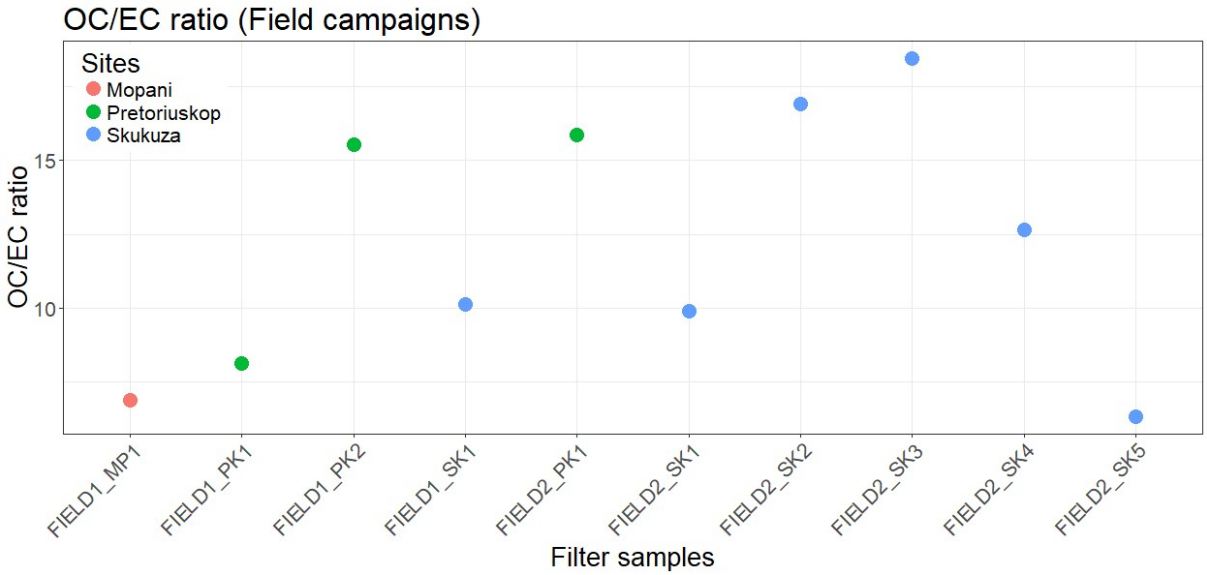

Figure 3-3. OC/EC ratio of the samples from field campaigns.

3.3 $\delta^{13}C$

3.3.1 ^{13}C signatures of raw biomass materials

Raw biomass material samples from each lab experiments are analyzed in the isotope laboratory at RUG and ^{13}C signature is measured. ^{13}C signature of both C_3 and C_4 biomass materials is shown in the table 3.1.

Table 3-2. $\delta^{13}C$ signatures of raw biomass samples burnt in the lab experiments

		$\delta^{13}C$				
Experiment #	**Samples**	**1st piece**	**2nd piece**	**3rd piece**	**4th piece**	**Average**
Lab-2 & 3	Corn	-12.64				-12.64
Lab-1, 2 & 3	Willow	-28.98				-28.98
Lab-1 & 2	Tinder	-25.65				-25.65
Lab-4 & 5	Wood	-27.22	-25.58	-26.78	-27.43	-26.75
Lab-4 & 5	Corn grain	-11.32	-11.39			-11.36
Lab-4 & 5	Corn leaf	-12.70	-12.52			-12.61

Raw biomass materials from few sites of field campaign in South Africa were collected and brought to the isotope laboratory for ^{13}C signature measurement. ^{13}C signature is shown in the table 3.2 and the figure 3.2.

Table 3-3. $\delta^{13}C$ signatures of raw biomass samples burnt in the field campaigns

Samples	$\delta^{13}C$			
	1st piece	**2nd piece**	**3rd piece**	**Average**
Mopane elephant dung	-21.203	-16.009	-23.171	-20.127
Mopane grass	-12.568	-13.162	-12.645	-12.792
Mopane leaves	-28.460	-28.685	-26.917	-28.021
Pretorius elephant dung	-15.248	-13.059	-13.462	-13.923
Pretorius grass	-13.251	-13.132	-12.589	-12.991
Pretorius mumbi	-27.440	-27.910	-27.302	-27.551
Satara grass	-13.114	-12.902	-12.725	-12.914

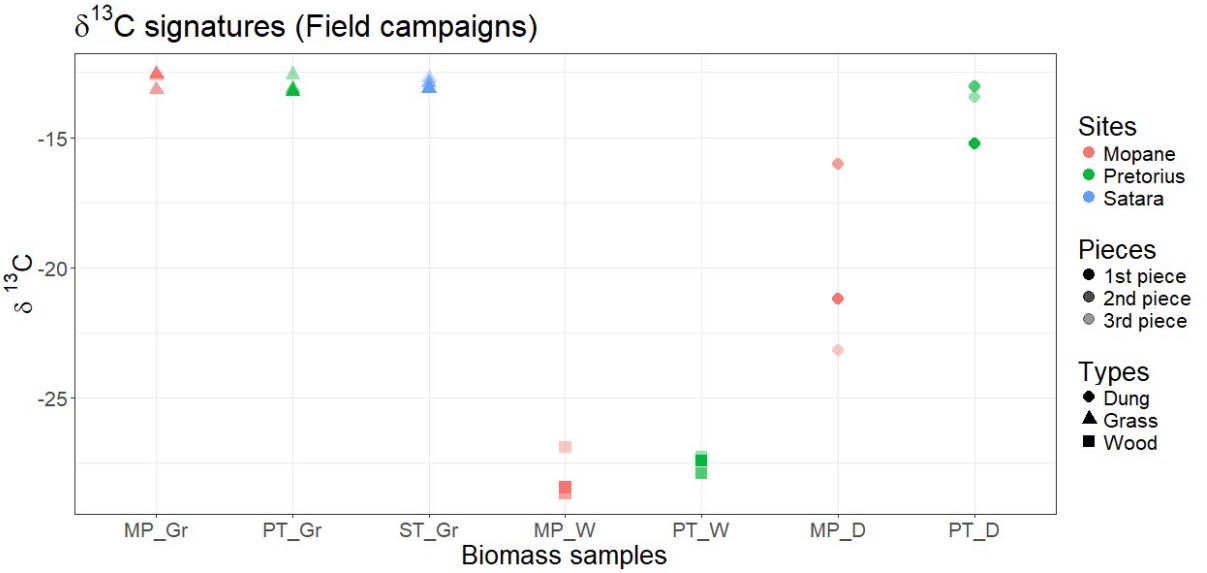

Figure 3-4. $\delta^{13}C$ signatures of raw biomass samples burnt in the field campaigns

3.3.2 $\delta^{13}C$ of OC of samples from C_3 (Willow) and C_4 (Corn) biomass burning

Three laboratory experiments were conducted in which pure C_3 and C_4 biomass was burned: first lab experiment (LE1), second lab experiment (LE2) and third lab experiment (LE3). In the 1st experiment, only willow materials were burned, whereas in the 2nd experiment, both corn and willow materials were burned separately. To start with a good flame, some tinder materials (very dry) were added too. And in the third experiment, willow materials, corn materials and their mixtures with different percentage were burned without tinder.

Fig. 3-3 and 3-4 show the $\delta^{13}C$ values of OC of the samples from two types of biomass burning (willow and corn respectively) in first three lab experiments. Both figures also contain ^{13}C signatures of raw biomass materials- willow and corn as the dotted line.

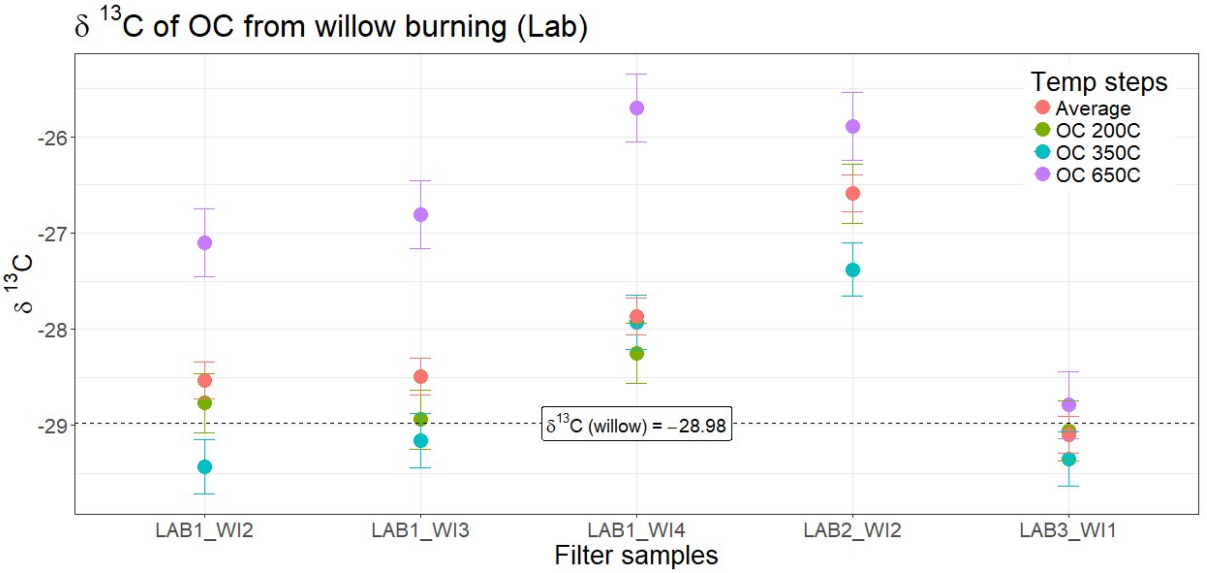

Figure 3-5. $\delta^{13}C$ of OC of the samples after burning willow materials in the lab experiments

From above graph, it can be found that weighted average $\delta^{13}C$ values of OC of the samples after burning willow materials are higher than the ^{13}C signature of willow for first two lab experiments. Also, for these two experiments, $\delta^{13}C$ values in 3rd temperature step (650C) is quite higher than 1st and 2nd temperature steps. On the other hand, for the third temperature step, the $\delta^{13}C$ values in three

temperatures steps as well as the weighted $\delta^{13}C$ values are quite close to the ^{13}C signature of willow. The possible reason of this can be the tinder materials with a ^{13}C signature of -25.65‰ mixed with willow materials during 1st and 2nd lab experiments.

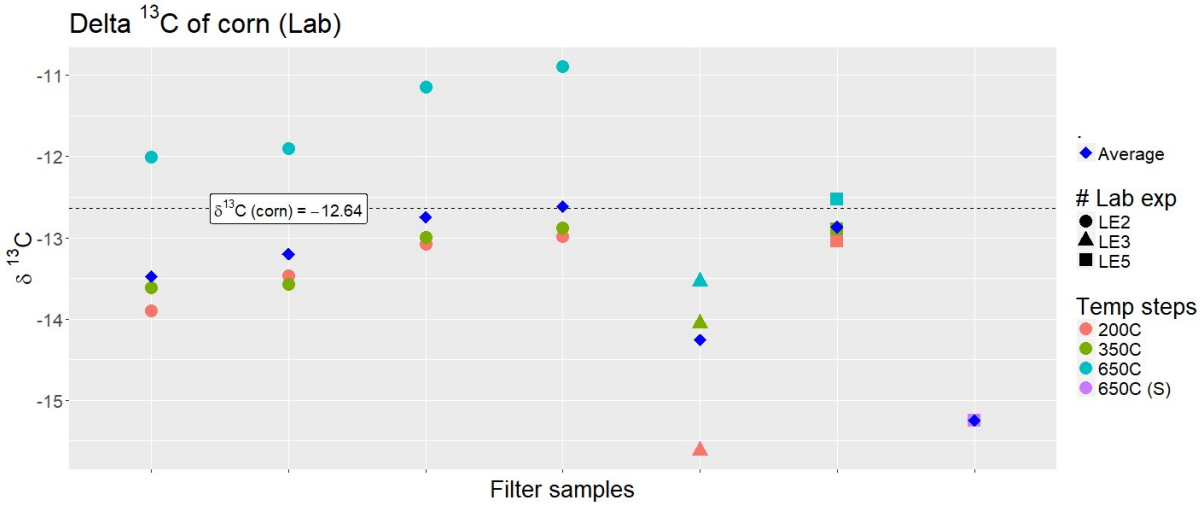

Figure 3-6. $\delta^{13}C$ of OC of the samples after burning corn materials in the lab experiments

From the graph in figure-3-3, it can be found that the weighted average $\delta^{13}C$ values of OC of the samples after burning corn materials are lower than the ^{13}C signature of corn for all three lab experiments (2nd, 3rd and 5th). Also, the $\delta^{13}C$ in 3rd temperature step (650C) is quite higher than 1st and 2nd temperature steps. Samples from 2nd experiment are more enriched than those from 3rd and 5th experiments, though the biomass burnt in 2nd experiment contains tinder materials which are more depleted than corn materials.

3.3.3 $\delta^{13}C$ of OC of samples from burning of mixtures of C_3 and C_4 biomasses

In 3rd experiment, mixtures of corn and willow with different proportion were burned. Everytime 500 gm biomass materials were burned with varying weighs of corn and willow. In the element analyzer, carbon content of corn and willow materials were measured and found that carbon content of both samples is almost similar. Carbon content of different parts of corn and willo materials is listed in the table: 3-3 and percentage of the carbon in corn in different mixtures is listed in the table: 3-4.

Table 3-4. Carbon contents of biomass samples (corn and willow)

	% C in Corn	% C in Willow
part-1	39.37	43.06
part-2	44.09	44.63
part-3	42.59	41.93
Average	42.02	43.21

Table 3-5. 3rd lab experiment: mixtures with different proportion of corn and willow

Corn (gm)	Willow (gm)	C in corn (gm)	C in willow (gm)	% corn carbon in mixture	Approximate proportion (%)
0	500	0.00	216.05	0.00	0
100	400	42.02	172.84	19.56	20
200	300	84.04	129.63	39.33	40
250	250	105.05	108.03	49.30	50
300	200	126.06	86.42	59.33	60
400	100	168.08	43.21	79.55	80
500	0	210.10	0.00	100.00	100

Figure:3-5 shows the $\delta^{13}C$ values of the samples collected from the burning of mixtures of corn and willow materials with different proportion. The figure also contains the ^{13}C signatures of raw corn and willow.

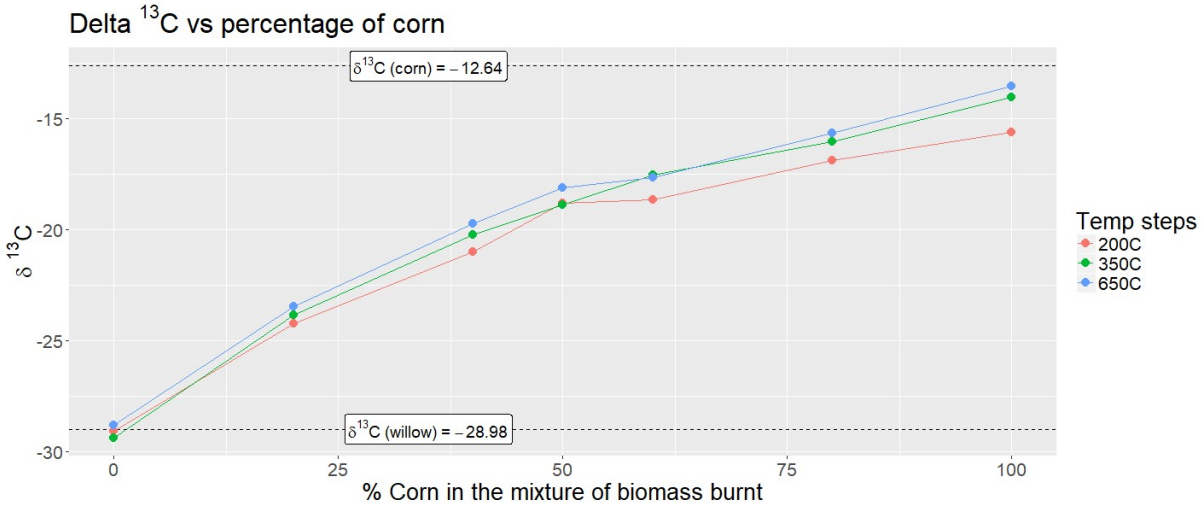

Figure 3-7. $\delta^{13}C$ values vs percentage of corn in the mixture of biomass burnt in lab experiment:3.

From the above figure, it can be found that sample from pure willow (100% willow, ie- 0% corn) has close $\delta^{13}C$ value to the ^{13}C signature of raw willow, where aerosol sample from pure corn (100%) is a bit depleted from raw biomass. While increasing the proportion of corn in the mixtures burnt, from 0% to 100%, the increase in the $\delta^{13}C$ values is not linear. Corn has higher contribution in $\delta^{13}C$. With 50%-50% mixture, $\delta^{13}C$ value is closer to the $\delta^{13}C$ of 100% corn than that of 100% willow.

3.3.4 $\delta^{13}C$ of Field campaign samples

Fig. 3-6 shows the $\delta^{13}C$ values of OC of the samples collected from the biomass burning in South Africa. Smples were collected in three sites: Mopani, Petoriuskop and Skuzua. Savanna grasses were burned along with wood branches and leaves of C_3 plants. Also, animal dung, specially elephant could be available among the burning materials. From the table 3-2 and fig. 3-2, it can be found that ^{13}C signature of grasses in all three sites are almost same, the average ^{13}C signature of grasses is -12.9‰. Leaves collected from Mopane site have the ^{13}C signature of -28.02‰ and wood collected from Petoriuskop site has ^{13}C signature of -27.55‰. Fig 3-6 also contains the average ^{13}C signatures of C_4 (grasses) and C_3 plants. ^{13}C signature of elephant dung varies in quite a long range mainly due to food habit to different types of plants, but the average value is close to ^{13}C signature C_4 plants (not shown in the fig. 3-6).

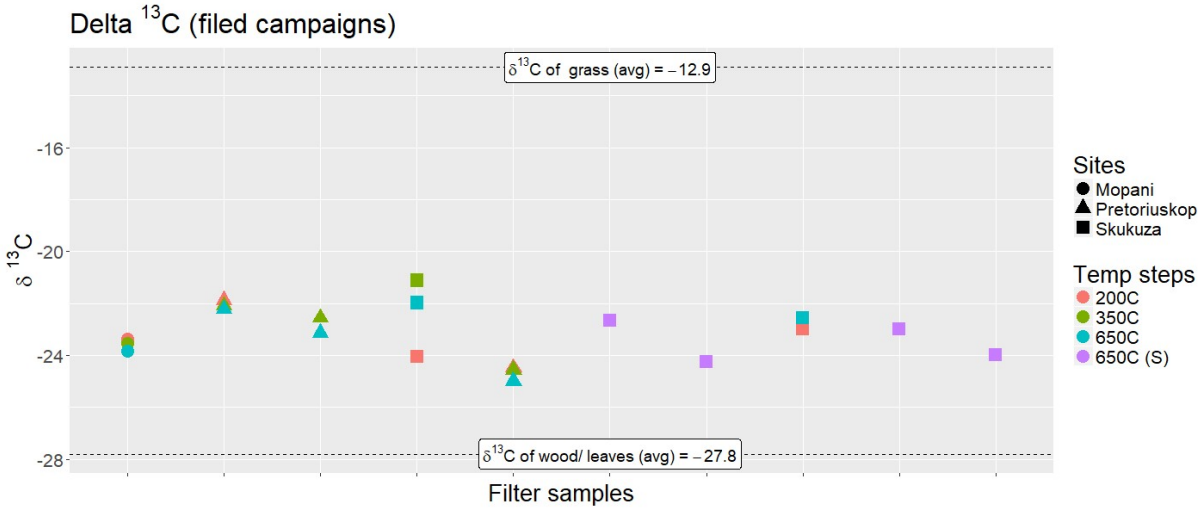

Figure 3-8. $\delta^{13}C$ values of OC of the samples from field campigns

The $\delta^{13}C$ value of OC of the samples from field campaigns varies from -24.98 to -21.11‰. The weighted average of $\delta^{13}C$ values in three temperature steps varies from -24.67 to -22.08‰. From the fig 3-6, it can be found that $\delta^{13}C$ values are more inclined to the ^{13}C signature of C_3 plants than that of C_4 plants. Though the all the burning plots contained lots of savanna grasses, there were tree branches and leaves as well. During the fire, savanna grasses were burned out very fast and rest of the time woody branches were burning. Biomasses were burned in the open field and most of the smoke was scattered in the air. Only a small portion of aerosol could be collected on the filters which were placed on top of the main flame. As the C_4 grasses were burned out very fast, aerosol produced by C_3 plants became prominent in the filter. This has been reflected in the $\delta^{13}C$ of OC of the samples from field campaigns.

3.3.5 $\delta^{13}C$ and modified combustion efficiency

Lab experiment: 4 and 5 were held in order to find the impact of burning condition on the $\delta^{13}C$. In lab experiment:4, C_3 materials (dry wood waste) and in lab experiment:5, C_4 materials (small pieces of corn) were burned. In each experiment, burning conditions were varied and modified combustion efficiency was calculated as per below equation:

$$\mathrm{MCE} = \frac{\Delta CO_2}{\Delta CO + \Delta CO_2} \quad (27)$$

Where, $\Delta CO_2/\Delta CO$ = average CO_2/CO in the smoke − background CO_2/CO in the lab air.

During the fires with corn materials in experiment:5, it was difficult to vary the burning condition, ie the MCE varied in quite a small range and it can be difficult draw any conclusion out of this. Therefore, only lab experiment-4, where dry wood waste was burned with different burning conditions, is used to find the possible impact of MCE on $\delta^{13}C$. Fig. 3-7 shows the $\delta^{13}C$ values of OC of samples after burning wood waste materials (C_3 plants) vs modified combustion efficiency. In this experiment, there were 6 fires, out of which 4 fires were with dry biomass and 2 with moisture added.

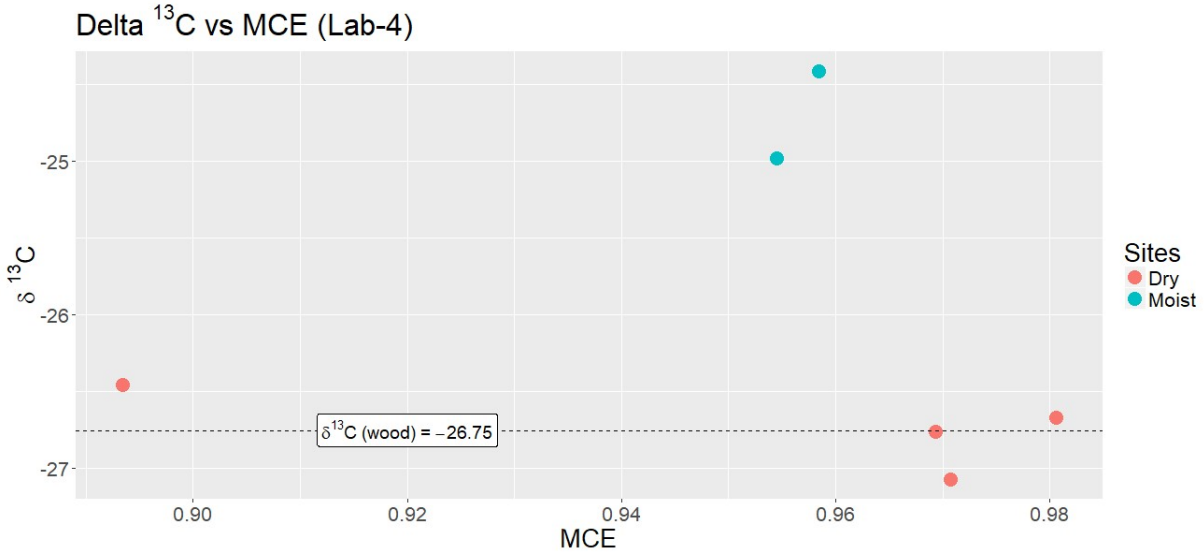

Figure 3-9. $\delta^{13}C$ values vs MCE of the samples from lab experiment-4.

From the above figure, there can be no strong evidence found for having impact of MCE on $\delta^{13}C$. But, the moisture seems to have a good impact on $\delta^{13}C$, though only two samples were collected with moisture added. Samples from burning moist biomass are more enriched than those from burning dry biomass. Also adding more moisture results in a higher $\delta^{13}C$. Though adding moisture caused more smogs and smokes (mainly water vapor), but MCE didn't vary much. Therefore, possible reason for this impact of moisture on $\delta^{13}C$ is that moisture can cause different parts of biomass to burn differently

and different parts of the same plant have different ^{13}C signatures. To find out the definite answer, further investigation is required.

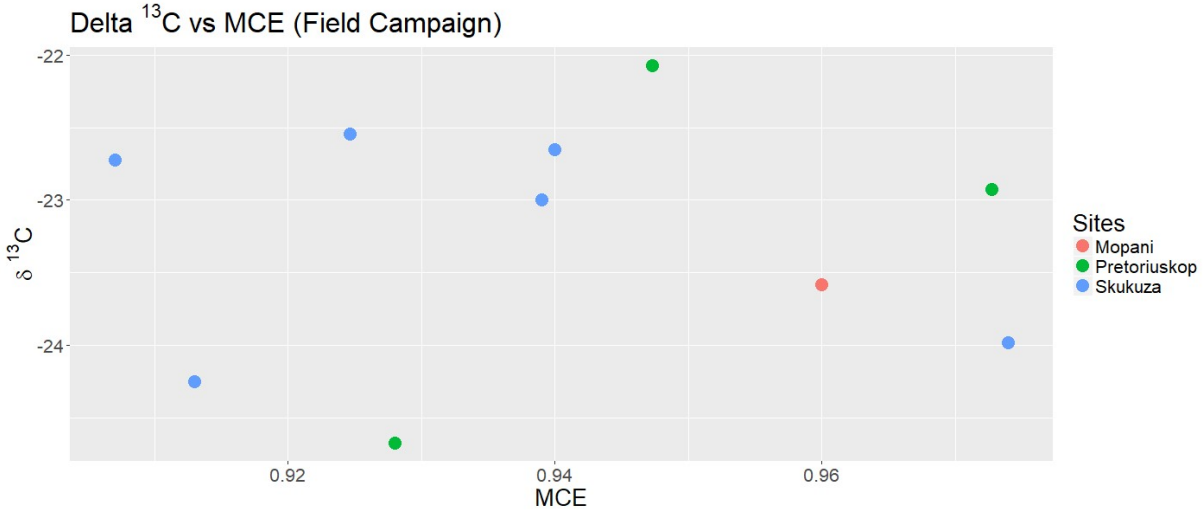

Figure 3-10. $\delta^{13}C$ values vs MCE of the samples from field campaigns.

Fig. 3-8 shows the graph of $\delta^{13}C$ values of OC of the samples from field campaigns in South Africa vs the modified combustion efficiency of each of the fires. From this scatter plot of $\delta^{13}C$ vs MCE, it can be found that $\delta^{13}C$ is randomly related to MCE.

3.4 Optical measurement

Transmittance signal of dark and white filter sample is measured during the measurement of OC/TC ratio (EUSAAR2 protocol). A selected area (1.5 cm^2) of the filter sample with aerosol collected on it (black filter) is placed into the front oven where it is exposed to a laser system and the transmittence signal is continuously recorded while the EUSAAR2 protocol is running. Initial reading of the transmittance signal represents the transmittance signal of dark filter (I_{Td}). During running the EUSAAR2 protocol, all the carbon content (both OC and EC) on the filter is volatilized and/or oxidized to CO_2 and at the end white filter is left. Last reading of the transmittance signal is regarded as the transmittance signal of white filter (I_{Tw}). The attenuation coefficients, $b_{ATN;Sunset}$ are calculated according the equation-20, where flow rate, Q of the aerosol pump during collection is: 3 L/m (0.00005 m^3/s) and the area of the filter sample exposed to aerosols is 0.000908 m^2 and 0.000363 m^2 for the filters with diameters of 37mm and 25mm respectively. To obtain absorption coefficient of aerosol sample, calibration is required.

3.4.1 Calibration

Lab experiment: 6 was held for the calibration between attenuation coefficient and absorption coefficient. Real time absorption coefficient was measured with the instrument - multi-angle absorption photometry (MAAP) while collecting the aerosol samples from biomass burning. MAAP instrument gives the data of black carbon (BC) concentration in ng/m3, from which babs;MAAP is calculated accroding to equation: $b_{abs;MAAP}$ = BC * MAE, where mass absorption efficiency (MAE) of MAAP is reported as 6.6 m^2/g. The attenuation coefficient, $b_{ATN;Sunset}$ of the same filter samples were obtained with the help of the Sunset carbon analyzer where transmittance signal of dark and white sample was measured. The BC concentration and absorption coefficient obtained from MAAP and the attenuation coefficient obtained with Sunset analyzer are listed in the table: 3.6.

Table 3-6. Calibration data of the samples from lab experiment:6

Filtername	Biomass	ΔATN	$b_{ATN;sunset}$ (m^{-1})	MAE (m^2/g)	BC MAAP (ng/m^3)	$b_{abs;MAAP}$ (m^{-1})
LAB6_WO1	Wood	0.09494	0.00044	6.6	17550.10	0.00012
LAB6_WO5	Wood	0.31985	0.00120	6.6	21170.62	0.00014
LAB6_WO6	Wood	0.30945	0.00123	6.6	36348.10	0.00024
LAB6_WC1	Wood chips	0.30626	0.00129	6.6	27166.93	0.00018
LAB6_H1	Hay	0.25923	0.00135	6.6	32527.94	0.00021
LAB6_H2	Hay	0.24665	0.00124	6.6	40490.06	0.00027
LAB6_WO8	Wood	0.14789	0.00073	6.6	44695.19	0.00029
LAB6_WO9	Wood	0.02488	0.00015	6.6	6380.57	0.00004
LAB6_WC2	Wood chips	0.14435	0.00073	6.6	31652.92	0.00021
LAB6_WC3	Wood chips	0.05247	0.00027	6.6	6046.32	0.00004
LAB6_WO7	Wood	0.30352	0.00122	6.6	40718.60	0.00027

Figure 3-11(a) shows the attenuation coefficient measured with Sunset carbon analyzer vsesus the absorption coefficient measured with the MAAP and the linear fit line of $b_{ATN;Sunset} = 3.55655 * b_{abs;MAAP}$. The linear regression of $b_{ATN;Sunset} \sim b_{abs;MAAP}$ gives the intercept = 0.00025 and slope = 3.55655, where the P-value of intercept is 0.33. Therefore, accepting the hypothesis that intercept = 0, mentioned regression equation is obtained. For each of the samples, the ratio between $b_{ATN;Sunset}$ and $b_{abs;MAAP}$ is calculated and plotted in the figure: 3-11(b). To parametrise, a simple funtion C.R(ΔATN) = C. Exp(b*ΔATN) has been chosen. The nonlinear regression equation as obtained from R is given by C.R(ΔATN) = 3.3441 * Exp(1.8796 * ΔATN) and the exponential fit line is also shown in the figure:3-11(b).

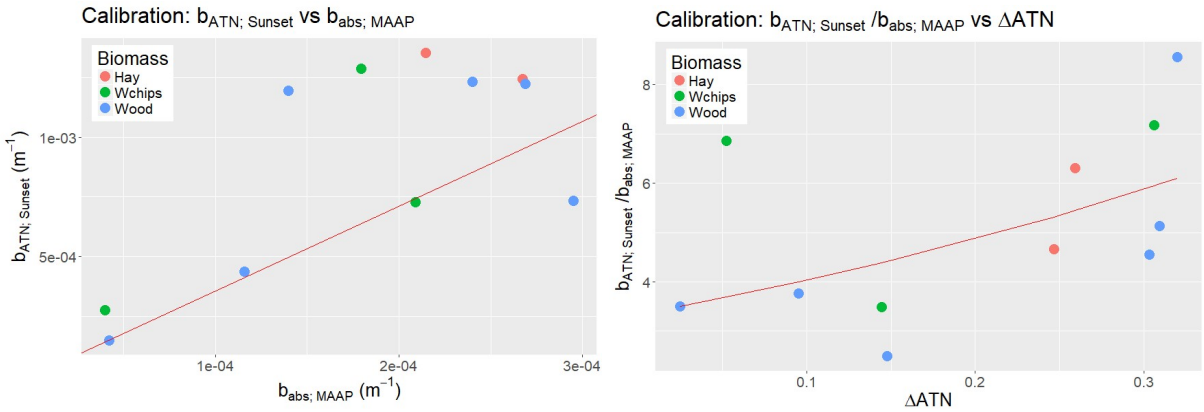

Figure 3-11. The results of calibration: (a) The attenuation coefficient measured with the Sunset carbon analyzer plotted versus the absorption coefficient measured with the MAAP and the linear fit line of $b_{ATN} = 3.5565 * b_{abs}$. (b) The ratio of attenuation coefficient with Sunset and abosrption coefficient with MAAP versus attenuation and the exponential fit line of C.R(ΔATN) = 3.3441 * exp(1.8796 * ΔATN)

From the calibration plots in figure:3-11, it can be found that both the linear and exponential fit lines are not well representative of the actual data points. Most of the data points are outside the fitlines and both the fits have high residual errors (0.0003355 & 1.688). Only 49.54% data points can be explained by the linear fit (R^2 = 0.4954). Therefore, the calibration is not fully successful and the calibration factor, C.R(ΔATN) obtained from this experiment is not trustworthy. The possible reason for this untrustworthy calibration can be the wrong handling of MAAP instrument. The number of samples is also low to get a good statistical analysis (only 11 data points). Moreover, some samples have very low carbon content and therefore the filters are almost blank with I_{Td} quite close to I_{Tw}.

3.4.2 Attenuation coefficients

Since the calibration was not successful, the absorption coefficients of the various samples have not been calculated with the untrustworthy calibration factor. Instead, the attenuation coefficients of the samples are examined as attenuation and absorption coefficients are linearly correlated to each other. The attenuation coefficients of all the samples from lab experiments (LAB:1 to LAB5) versus elemental carbon (EC) content on the filter (µg/cm^2) is plotted in the figure:3-12 (a). From the plot it can be found that attenuation coefficient of the different samples is mostly dependent on the EC content on the filter. The plot hardly shows any relation between attenuation coefficients and biomass burnt. However, in order to get this relation data from lab experiment:3 has been examined where mixtures of corn and willow with different proportion were burned. Figure:3-12(b) shows the graph of the attenuation coefficients of samples from lab experiment:3 vs percentage of corn content in the biomass mixtures. From the plot it can be found that the attenuation coefficient decreases if percentage of corn in the biomass mixture increases. This can be explained by the fact that OC/EC ratio for corn is much higher than that for willow and the ratio increases (and EC decreases) with the increase of the percentage of corn in the mixture. However, this relation is found for corn and willow burn in the plot 3-12(a) because corn and willow (and other biomasses) were burned in different experiments with different conditions (combustion conditions, duration of the fire etc).

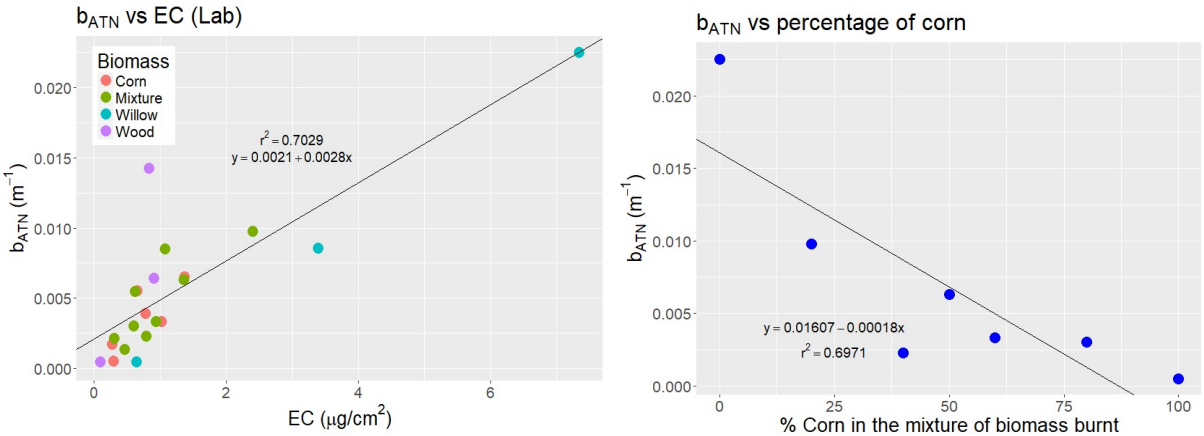

Figure 3-12. Attenuation coefficient measured with Sunset. a) Attenuation coefficients vs EC (m^2/g) of lab experiments. b) Attenuation coefficient vs percentage of corn in the mixture of biomass burnt in lab experiment:3

Figure:3-13 shows the attenuation coefficients of the samples from field experiments versus the elemental carbon (EC) on the filter samples (µg/cm^2). From this figure, it can be found that the attenuation coefficient is quite linearly correlated with elemental carbon on the filters for Skukuza and Mopani sites. For Pretoriuskop site, the data points (only two) show different pattern from other two sites.

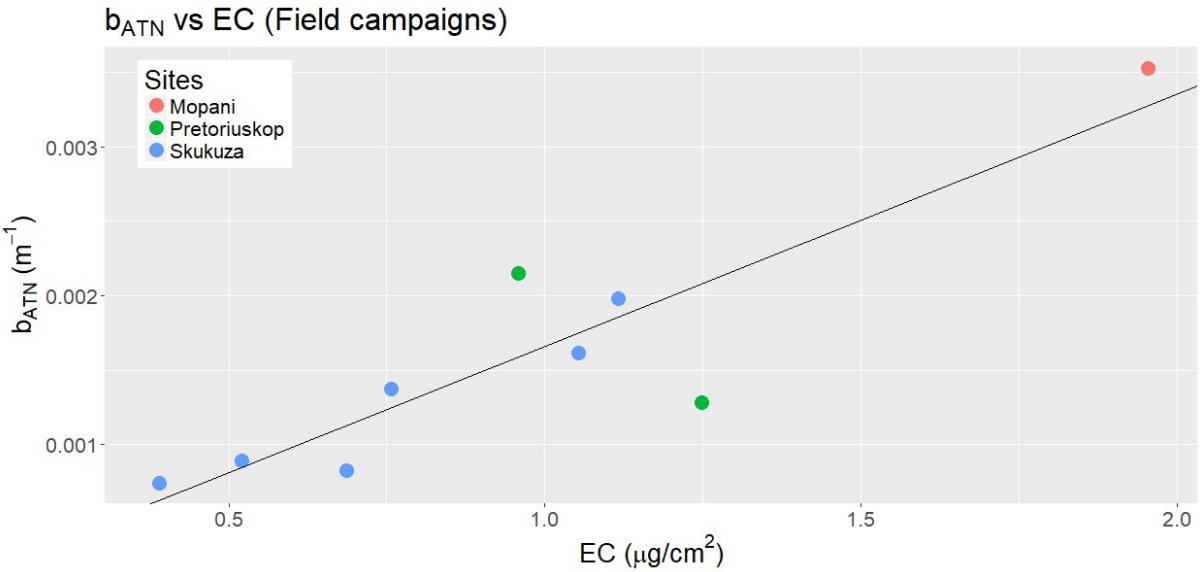

Figure 3-13. Attenuation coefficient of samples from field campaigns versus EC

4. CONCLUSION AND DISCUSSION

The goal of this research project was to characterize the aerosol samples from biomass burning in terms of $\delta^{13}C$ values of OC, OC/EC ratio and optical measurements. Samples were collected from two field experiments as well as six laboratory experiments and then analyzed. Analysis of the aerosol samples from lab experiments is used to characterize the aerosol samples from field experiment.

In the lab experiments 1, 2 and 3 branches of willow tree were burned and corn was burned in experiments 2, 3 and 4. The results show that organic carbon (OC) from combustion of willow or corn shows $\delta^{13}C$ comparable to the burnt plant material. For combustion of willow (C_3), the $\delta^{13}C$ values in OC tend to be slightly higher than in the fuel, whereas for combustion of corn $\delta^{13}C$ of OC tend to be slightly lower than in the fuel. In experiment 3, mixtures of corn and willow materials with different proportions were burned. For mixtures of willow and corn, the relationship between $\delta^{13}C$ in the emitted organic carbon and the fuel mixture is slightly non-linear: For a 50-50% willow and corn mixture, the $\delta^{13}C$ in OC is closer to that of corn than that of willow. Results of $\delta^{13}C$ values of OC in three temperature steps (200C, 450C and 650C) show that $\delta^{13}C$ of OC volatalized in 650C is higher than that of OC volatalized in 200C and 350C. This happend for both lab and field experiments, for burning of C_3 & C_4 plants and their mixtures.

The field experiment results show that $\delta^{13}C$ values of OC are in the range of -21.11‰ to -24.98‰ where average ^{13}C signatures of C_3 and C_4 fuel collected from the sites are -27.8‰ and -12.9‰ respectively. This gives the possibility of burning of mixtures both of C_3 and C_4 plants with higher contribution from C_3 plants. During the field experiments several plots of mainly savanna grasses (specially in Skukuza and Petroiuskop sites) were burned along with dry tree leaves, few woody trees and bushes. Therefore, more contribution from the C_4 was expected in $\delta^{13}C$ values of OC. The possible reasons of higher contribution in $\delta^{13}C$ of OC from C_3 plants can be that savanna grass is lighter than C_3 wood, savanna grasses burn much faster than C_3 wood and due to collection of aerosol in open field, lower fraction of aerosols from grasses in more spreaded field can be collected than aerosols from few wood trees. To get a definitive reason, further investigation will be useful about study of the fires, approximate mass ratio of burning materials, burning conditions, etc. Also, investigation of the samples from burning of C_3 and C_4 seperately will help to characterize the aerosols more precisely.

Modified combustion efficiency (MCE) for both the lab and field experiments seems to have no impact upon the $\delta^{13}C$ since $\delta^{13}C$ and MCE are found randomly distributed. But, from this research it can't be claimed that there is no impact of combustion efficiency on $\delta^{13}C$, because all the experiments have quite a low range of MCE and only a small number of fires with same fuel could be possible. Therefore, further investigation is required. In the lab experiment 4 moisture was added to the fuel in order to vary the MCE. The results show an interesting finding though only two samples were collected with added moisture. Moisture shows a significant impact on the $\delta^{13}C$: the $\delta^{13}C$ in OC from moist wood tend to be slightly higher than from dry wood. Possible reason for this impact of moisture on $\delta^{13}C$ is that moisture can cause different parts of biomass to burn differently and different parts of the same plant have different ^{13}C signatures. To find out the definite answer, further investigation is required.

OC/EC ratio of the samples from corn burning is found much higher than that from willow or wood chips burning. Depending upon combustion condition, combustion duration, moisture etc OC/EC ratio varies in a quite large range: from 4.7 to 37.7 for samples from willow/ wood burning and from 44.7 to 112.4 for samples from corn burning. The proportion of corn and willow in biomass mixtures burnt shows a linear relation with OC/EC ratio. An increment in the percentage of corn in the biomass mixtures increases the OC/EC ratio of the aerosol samples. Since corn contributes much more than willow to the organic carbon (OC), it has higher contribution in $\delta^{13}C$ as well, ie with 50%-50% mixture, $\delta^{13}C$ value is closer to the $\delta^{13}C$ of 100% corn. The samples from the biomass burning in the field

experiments have the OC/EC ratio in the reange from 6.3 to 18.5. Since the OC/EC ratio of the aerosols from individual burning of C_3 and C_4 plants in the plots of field experiments, is unknown, it is not possible to find which plants have higher contribution to these samples. Further fire experiments of individual biomass would be useful.

Calibration factor betweem absorption coefficient measured with Sunset carbon analyzer and attenuation coefficient measured with MAAP was not statistically reliable and it was not furthered used for the calculation of absorption coefficients and mass absorption efficiency (MAE) of EC. The attenuation coefficients of the samples from different lab experiments and field experiments generally show linear relation with elemental carbon (EC) on the filter sample as expected since higher EC is responsible for more attenuation.

Many filter samples of field and lab experiments contained very low amount of total carbon and measurement of these filters may give unreliable results. Some of the filters contained too little carbon content (almost blank) to be used for further measurements and thus data points in the analysis decreased. A pump with higher flow rate would be used and/ or more samples would be collected considering a portion of unmeasurable samples while planning for the furher experiments.

5. BIBLIOGRAPHY

Ammerlaan, B., R. Holzinger, A. Jedynska, and J. Henzing. 2017. "Technical note: Aerosol light absorption measurements with a carbon analyzer - calibration and precision estimates." *Atmospheric Environment 164 (2017) 1-7* (Atmospheric Environment 164).

Andreae, M. O., and P. Merlet. 2001. "Emission of trace gases and aerosols from biomass burning ." *GLOBAL BIOGEOCHEMICAL CYCLES, VOL. 15, NO. 4, PAGES 955-966.*

Ballentine, D. C., S. A., Macko, and V. C. Turekian. 1998. "Variability of stable carbon isotopic compositions in individual fatty acids from combustion of C_3 and C_4 plants: implications for biomass burning." *Chemical Geology 152 (1998) 151–161.*

Ballentine, Donna C., Stephen A. Macko, Vaughan C. Turekian, William P. Gilhooly, and Bice Martincgh. 1996. "Compound specific isotope analysis of fatty acids and polycycfic aromatic hydrocarbons in aerosols: impfications for biomass burning." *Organic Geochemistry, Vol. 25, No. 1/2, pp. 97-104.*

Bond, Tami C., David G. Streets, Kristen F. Yarber, Sibyl M. Nelson, Jung-Hun Woo, and Zbigniew Klimont. 2004. "A technology-based global inventory of black and organic carbon." *JOURNAL OF GEOPHYSICAL RESEARCH, VOL. 109, D14203, doi:10.1029/2003JD003697.*

Brand, W. A., S. S. Assonov, and T. B. Coplen. 2010. "Correction for the ^{17}O interference in $\delta(^{13}C)$ measurements when analyzing CO_2 with stable isotope mass spectrometry (iupac technical report)." *Pure and Applied Chemistry_ January 2010. DOI: 10.1351/PAC-REP-09-01-05.*

Cavalli, F., M. Viana, K. E. Yttri, J. Genberg, and J.-P. Putaud. 2010. "Toward a standardised thermal-optical protocol for measuring atmospheric organic and elemental carbon: the eusaar protocol." *Atmospheric Measurement Techniques, 3, 79–89.*

Chen, J., C. Lia, Z. Ristovski, A. Milic, Y. Gub, M. S. Islam, S. Wangc, et al. 2017. "A review of biomass burning: Emissions and impacts on air quality, health and climate in china. ." *Science of The Total Environment, Volume 579,* 1000–1034.

Dusek, U., C. Meusinger, B. Oyama, W. Ramon, P. de Wilde, R. Holzinger, and T. Röckmann. 2013. "A thermal desorption system for measuring $\delta^{13}C$ ratios on organic aerosol." *Journal of Aerosol Science. 66 (2013) 72–82.*

Garbaras, A., A. Masalaite, I. Garbariene, D. Ceburnis, E. Krugly, V. Remeikis, E. Puida, K. Kvietkus, and D. Martuzevicius. 2015. "Stable carbon fractionation in size-segregated aerosol particles produced by controlled biomass burning." *Journal of Aerosol Science 79 (2015) 86–96.*

Hobbie, Erik A., and Roland A. Werner. 2004. "Intramolecular, compound-specific, and bulk carbon isotope patterns in C_3 and C_4 plants: a review and synthesis." *New Phytologist (2004) 161: 371–385.*

Mašalaitė, A., A. Garbaras, and V. Remeikis. 2012. "STABLE ISOTOPES IN ENVIRONMENTAL INVESTIGATIONS." *Lithuanian Journal of Physics, Vol. 52, No. 3, pp. 261–268 (2012).*

Monson, Russell K., Gerald E. Edwards, and Maurice S. B. Ku. 1984. "C_3-C_4 Intermediate Photosynthesis in Plants." *BioScience, Volume 34, Issue 9, October 1984, Pages 563–574, https://doi.org/10.2307/1309599.*

Moosmuuller, H., R.K. Chakrabarty, and W.P. Arnott. 2009. "Aerosol light absorption and its measurement: A review." *Journal of Quantitative Spectroscopy & Radiative Transfer 110* 844–878.

Ni, H., R.-J. Huang, J. Cao, T. Zhang, M. Wang, H. A. Meijer, and U. Dusek. 2018. "Source apportionment of carbonaceous aer osols in xi'an, china: insights from a full year of

measurements of radiocarbon and the stable isotope ^{13}C." *Atmospheric Chemistry and Physics Discussions., https: // doi. org/ 10. 5194/acp-2018-130.*

Petzold, A., J. A. Ogren, M. Fiebig, P. Laj, S.-M. Li, U. Baltensperger, T. Holzer-Popp, et al. 2013. "Recommendations for reporting “black carbon” measurements." *Atmospheric Chemistry and Physics, 13, 8365–8379, 2013. doi:10.5194/acp-13-8365-2013.*

Petzolda, Andreas, and Markus Schonlinner. 2004. "Multi-angle absorption photometry - a new method for the measurement of aerosol light absorption and atmospheric black carbon." *Aerosol Science 35 (2004) 421–441.*

Poschl, U. 2005. "Atmospheric aerosols: Composition, transformation, climate and health effects." *Atmospheric Chemistry. DOI: 10.1002/anie.200501122.*

Roberts, G., M. J. W., and E. Lagoudakis. 2009. "Annual and diurnal African biomass burning temporal dynamics." *Biogeosciences, 6, 849–866.*

Seinfeld, J. H., and S. N. Pandis. 1998. "Atmospheric trace constituents, Chapter 2." In *Atmospheric chemistry and physics: From air pollution to climate change, 3rd edition*. John Wiley & Sons, Inc. ISBN: 978-1-118-94740-1.

Weingartner, E., H. Saatho, M. Schnaiter, N. Streit, B. Bitnar, and U. Baltensperger. 2003. "Absorption of light by soot particles: determination of the absorption coe%cient by means of aethalometers." *Aerosol Science 34 (2003) 1445–1463.*

Weingartnera, E., H. Saatho, M. Schnaiterb, N. Streita, B. Bitnarc, and U. Baltenspergera. 2003. "Absorption of light by soot particles: determination of the absorption coe%cient by means of aethalometers ." *Aerosol Science 34 (2003) 1445–1463.*

Werf, Guido R. van der, James T. Randerson, Louis Giglio, G. James Collatz, Mingquan Mu, Prasad S. Kasibhatla, Douglas C. Morton, Ruth S. DeFries, Yufang Jin, and Thijs T. van Leeuwen. 2010. "Global fire emissions and the contribution of deforestation, savanna, forest, agricultural, and peat fires (1997-2009)." *Atmos. Chem. Phys., 10, 11707-11735, https://doi.org/10.5194/acp-10-11707-2010.*

Williams, Jason E., Michiel van Weele, Peter F. J. van Velthoven, Marinus P. Scheele, Catherine Liousse, and Guido R. van der Werf. 2012. "The Impact of Uncertainties in African Biomass Burning Emission Estimates on Modeling Global Air Quality, Long Range Transport and Tropospheric Chemical Lifetimes." *Atmosphere 2012, 3, 132-163; doi:10.3390/atmos3010132.*